



Centralized training with hybrid execution in multi-agent reinforcement learning via predictive observation imputation

Pedro P. Santos^{a,b,^{ID},*}, Diogo S. Carvalho^{a,b,^{ID}}, Miguel Vasco^{c,^{ID}},
Alberto Sardinha^{d,^{ID}}, Pedro A. Santos^{a,b,^{ID}}, Ana Paiva^{a,b,^{ID}}, Francisco S. Melo^{a,b,^{ID}}

^a INESC-ID, Lisbon, Portugal

^b Instituto Superior Técnico, Lisbon, Portugal

^c KTH Royal Institute of Technology, Stockholm, Sweden

^d Pontifical Catholic University of Rio de Janeiro, Rio de Janeiro, Brazil

ARTICLE INFO

Keywords:

Multi-agent reinforcement learning
Reinforcement learning
Multi-agent systems
Machine learning

ABSTRACT

We study *hybrid execution* in multi-agent reinforcement learning (MARL), a paradigm where agents aim to complete cooperative tasks with arbitrary communication levels at execution time by taking advantage of information-sharing among the agents. Under hybrid execution, the communication level can range from a setting in which no communication is allowed between agents (fully decentralized), to a setting featuring full communication (fully centralized), but the agents do not know beforehand which communication level they will encounter at execution time. We contribute MARO, an approach that makes use of an auto-regressive predictive model, trained in a centralized manner, to estimate missing agents' observations at execution time. We evaluate MARO on standard scenarios and extensions of previous benchmarks tailored to emphasize the impact of partial observability in MARL. Experimental results show that our method consistently outperforms relevant baselines, allowing agents to act with faulty communication while successfully exploiting shared information.

1. Introduction

Multi-agent reinforcement learning (MARL) endeavors to acquire behavior that maximizes utility in scenarios involving multiple agents. Over recent years, deep MARL techniques have been effectively applied in various multi-agent domains such as game-playing [1], traffic light control [2], and energy management [3]. Despite recent accomplishments, the multi-agent setting presents significant challenges compared to its single-agent counterpart [4]: concurrent learners introduce non-stationarity conditions that hinder learning progress; the curse of dimensionality complicates centralized MARL approaches due to the exponential expansion of state and action spaces with the agent count; moreover, agents rarely observe the true environment state.

To address the challenge posed by the exponential growth in state/action space and environmental constraints, particularly in perception and actuation, current approaches focus on learning decentralized policies. These policies enable agents to make decisions based on local perceptions and partial knowledge of other agents' intentions. The concept of *centralized training with decentralized*

* Corresponding author.

E-mail address: pedro.pinto.santos@tecnico.ulisboa.pt (P.P. Santos).

<https://doi.org/10.1016/j.artint.2025.104404>

Received 16 February 2024; Received in revised form 13 August 2025; Accepted 16 August 2025

Available online 10 September 2025

0004-3702/© 2025 The Author(s). Published by Elsevier B.V. This is an open access article under the CC BY-NC license (<http://creativecommons.org/licenses/by-nc/4.0/>).

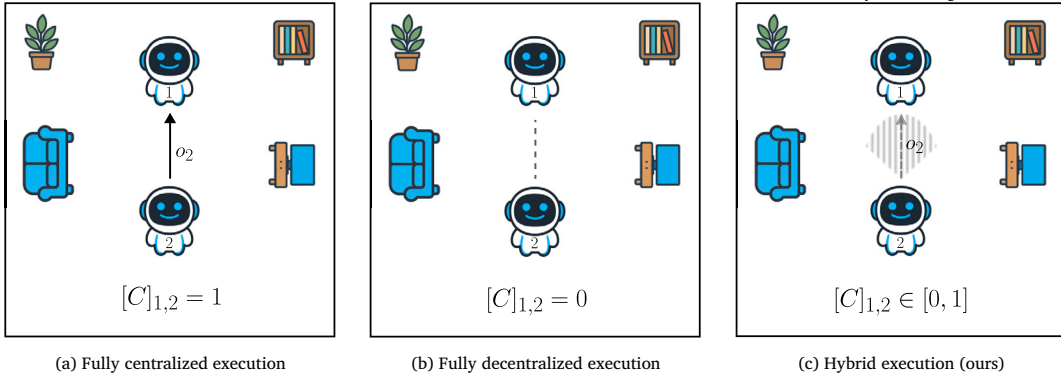


Fig. 1. Hybrid execution in MARL: we consider multi-agent systems that perform cooperative tasks under partial observability by passively sharing their observations o . During execution, agents act with arbitrary (but unknown) communication levels that are dictated by a communication matrix C (c); communication levels can range from full decentralization (b), where C is the identity matrix, to full centralization (a), where C is a matrix of ones.

execution stands as a cornerstone in recent research in the field [5–7]. This paradigm capitalizes on the availability of additional information solely during training, allowing the learning of decentralized policies without relying heavily on communication channels.

In certain scenarios, the need for partially observable environments and communication limitations necessitates the learning of entirely decentralized policies. However, imposing the assumption that agents cannot communicate during execution proves overly stringent for numerous real-world applications such as robotics, game-playing, and autonomous driving [8,9]. In such domains, adopting fully decentralized policies may prove overly restrictive, as they overlook the potential for inter-agent communication. Alternative MARL approaches that harness shared information among agents can undoubtedly be explored [10].

In this work, we focus our attention to the recently introduced paradigm of *centralized training with hybrid execution* [11]. We propose RL agents that are able to exploit the benefits of centralized training while, simultaneously, taking advantage of information-sharing at execution time. Under *hybrid execution* (Fig. 1), agents act in scenarios with arbitrary (but unknown) communication levels that can range from no communication (fully decentralized) to full communication between the agents (fully centralized). In particular, we consider scenarios with faulty communication during execution, in which agents passively share their local observations to perform partially observable cooperative tasks. We propose *multi-agent reconstruction of observations* (MARO), a novel method that allows agents to solve RL tasks regardless of the communication process encountered at execution time. MARO can be easily integrated with current deep MARL methods and comprises an auto-regressive model, trained in a centralized manner, that explicitly predicts non-shared information from past observations of the agents.

We evaluate the performance of MARO across different communication levels, in different MARL benchmark environments and using multiple RL algorithms. Furthermore, we introduce novel MARL environments that explicitly require communication during execution to successfully perform cooperative tasks, currently missing in the literature. Experimental results show that our method consistently outperforms the baselines, allowing agents to exploit shared information during execution and perform tasks under various communication levels.

In summary, our contributions are: (i) we contribute MARO, an approach that makes use of an autoregressive predictive model of agents' observations; and (ii) we evaluate MARO in multiple environments using different RL algorithms, showing that our approach consistently allows agents to act with different communication levels while outperforming relevant baselines.

2. Hybrid execution in multi-agent RL

A fully cooperative multi-agent system with Markovian dynamics can be modeled as a decentralized partially observable Markov decision process (Dec-POMDP) [12]. A Dec-POMDP is a tuple

$$([n], \mathcal{X}, \mathcal{A}, \mathcal{P}, \mathcal{P}_0, r, \gamma, \mathcal{Z}, \mathcal{O}),$$

where $[n] = \{1, \dots, n\}$ is the set of indexes of n agents, \mathcal{X} is the set of states of the environment, $\mathcal{A} = \times_i \mathcal{A}_i$ is the set of joint actions, where \mathcal{A}_i is the set of individual actions of agent i , \mathcal{P} is the set of probability distributions over next states in \mathcal{X} , one for each state and action in $\mathcal{X} \times \mathcal{A}$, \mathcal{P}_0 is the distribution over initial states, $r : \mathcal{X} \times \mathcal{A} \rightarrow \mathbb{R}$ maps states and actions to expected rewards, $\gamma \in [0, 1]$ is a discount factor, $\mathcal{Z} = \times_i \mathcal{Z}_i$ is the set of joint observations, where \mathcal{Z}_i is the set of local observations of agent i , and \mathcal{O} is the set of probability distributions over joint observations in \mathcal{Z} , one for each state and action in $\mathcal{X} \times \mathcal{A}$. A decentralized policy for agent i is $\pi_i : \mathcal{Z}_i \rightarrow \mathcal{A}_i$ and the joint decentralized policy is $\pi : \mathcal{Z} \rightarrow \mathcal{A}$ such that $\pi(z_1, \dots, z_n) = (\pi_1(z_1), \dots, \pi_n(z_n))$.

Fully decentralized approaches to MARL directly apply standard single-agent RL algorithms for learning each agent's policy π_i in a decentralized manner. In independent Q -learning (IQ-L) [13], each agent treats other agents as being part of the environment, ignoring the influence of other agents' observations and actions. Similarly, independent proximal policy optimization (IPPO), an adaptation of the PPO algorithm [14], learns fully decentralized critic and actor networks, neglecting the influence of other agents. More recently, under the paradigm of centralized training with decentralized execution, QMIX [6] aims at learning decentralized policies with centralization at training time while fostering cooperation among the agents. Multi-agent PPO (MAPPO) [15] learns

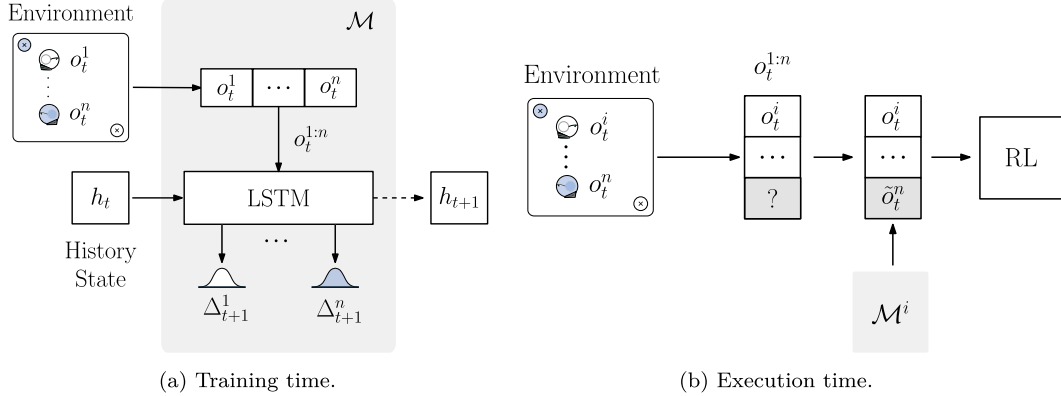


Fig. 2. MARO approach for hybrid execution: (a) at training time, an autoregressive predictive model \mathcal{M} learns to estimate observation deltas $p(\Delta_{t-1}^{1:n} | o_1^{1:n}, h_t)$ from previous observations $o_1^{1:n}$ and a history variable h_t ; and (b) at execution time, an agent-specific predictive model, \mathcal{M}^i , predicts missing agents' observations.

decentralized actors using a centralized critic during training. Finally, if we know that all agents can share their local observations among themselves at execution time, we can use any of the approaches above to learn fully centralized policies.

However, none of the previously mentioned methods accounts for scenarios where agents may intermittently access other agents' observations. Consequently, decentralized agents are unable to utilize additional information they might receive during execution, while centralized agents are incapacitated when information sharing fails. In this study, we focus our attention to hybrid execution in MARL, where agents act regardless of the communication process but aim to take advantage of any additional information they may receive during execution.

2.1. Hybrid partially observable Markov decision processes

As introduced in [11], the paradigm of centralized training with hybrid execution can be formalized under a class of multi-agent POMDPs termed hybrid-POMDPs (H-POMDPs). H-POMDPs explicitly model the communication process among agents and are defined as a tuple

$$([n], \mathcal{X}, \mathcal{A}, \mathcal{P}, \mathcal{P}_0, r, \gamma, \mathcal{Z}, \mathcal{O}, C)$$

where, in addition to the tuple that describes the Dec-POMDP, we consider a $n \times n$ communication matrix C such that $[C]_{i,j} = p_{i,j}$ is the probability that, at a certain time step, agent i has access to the local observation of agent j in \mathcal{Z}_j . H-POMDPs generalize both the notion of decentralized execution and centralized execution in MARL. Specifically, for a given Dec-POMDP, we can consider C as the identity matrix to capture fully decentralized execution or as a matrix of ones to capture fully centralized execution.

In our setting, we assume that at execution time agents will face an H-POMDP with an unknown communication matrix C , sampled from a set \mathcal{C} according to an unknown probability distribution μ . The performance of the agent is measured as $J_\mu(\pi) = \mathbb{E}_{C \sim \mu} [J(\pi; C)]$, where $J(\pi; C)$ denotes the expected discounted cumulative reward of policy π under an H-POMDP with communication matrix C . At training time, the agents have access to the fully centralized H-POMDP. Thus, the setting we consider is one of centralized training with *hybrid* execution and an unknown communication process. We seek to find a method that takes explicit advantage of the characteristics of hybrid execution to be able to act on H-POMDPs regardless of the matrix C that models the communication process at execution time.

3. Multi-agent observation sharing under communication dropout

While acting on an H-POMDP, agents may not have access to the perceptual information of all agents due to a faulty communication process. We propose *multi-agent reconstruction of observations* (MARO), an approach to exploit shared information and overcome communication issues during task execution. MARO comprises an autoregressive predictive model that estimates missing information.

We set up the RL controller of each agent, i.e., the Q -network associated with each agent for the IQN and QMIX algorithms, and the actor network associated with each agent for the IPPO and MAPPO algorithms, to receive as input the joint observation $o_t^{1:n} = \{o_t^1, \dots, o_t^n\}$, where o_t^i is the observation of the i -th agent at timestep t . In order to overcome communication failures during execution, we train a predictive model \mathcal{M} to impute the non-shared observations \tilde{o}_t^i , $i \in [n]$.

Training time We learn a transition model, $p(\Delta_t^{1:n} | o_t^{1:n}, h_t)$, depicted in Fig. 2a, that given the current observations $o_t^{1:n}$ and some history variable h_t is able to predict the next-step observations as $o_{t+1}^{1:n} = o_t^{1:n} + \Delta_t^{1:n}$, where $\Delta_t^{1:n}$ corresponds to the predicted deltas of the observations. We chose to predict observation deltas rather than raw observations as this approach has been successfully used in prior work on trajectory prediction [16]. We learn a single predictive model in a fully centralized and supervised fashion. We instantiate $p_\theta(\Delta_t^{1:n} | o_t^{1:n}, h_t)$ as an LSTM, parameterized by θ , with:

$$p_{\theta}(\Delta_t^{1:n} | o_t^{1:n}, h_t) = \prod_{i=1}^n p_{\theta}(\Delta_t^i | o_t^{1:n}, h_t), \quad (1)$$

where $p_{\theta}(\Delta_t^i | o_t^{1:n}, h_t)$ is the Gaussian distribution of the predicted deltas for the i -th agent. We train the predictive model and RL controllers simultaneously: we consider single-step transitions $(o_t^{1:n}, \Delta_t^{1:n})$, with $\Delta_t^{1:n} = o_{t+1}^{1:n} - o_t^{1:n}$, and evaluate the negative log-likelihood of the target next-step deltas $\Delta_t^{1:n}$, given the estimated next-step deltas distribution $p_{\theta}(\cdot | o_t^{1:n}, h_t)$:

$$\mathcal{L}_{\mathcal{M}}(o_t^{1:n}, \Delta_t^{1:n}) = - \sum_{i=1}^n \log p_{\theta}(\Delta_t^i | o_t^{1:n}, h_t). \quad (2)$$

Execution time During execution, we provide each agent with an independent instance of the predictive model \mathcal{M}^i , which updates the estimated joint-observations in the perspective of the agent $\tilde{o}_t^{1:n,i} = \{\tilde{o}_t^{1,i}, \dots, \tilde{o}_t^{n,i}\}$ and maintains an agent-specific history state h_t^i . As depicted in Fig. 2b, we use the predictive model \mathcal{M}^i to impute missing observations.

4. Evaluation

We evaluate our approach for hybrid execution against relevant baselines under multiple MARL algorithms. We show that the core component of MARO, i.e., the predictive model, allows the execution of tasks across multiple communication levels, outperforming baselines. We describe our experimental scenarios and baselines in Section 4.1 and Section 4.2, respectively. In Section 4.3, we present our main experimental results.

4.1. Experimental scenarios

We focus our evaluation on multi-agent cooperative environments. As discussed by [17], the main challenges in current MARL benchmark scenarios majorly involve coordination, large action space, sparse reward, and non-stationarity. Thus, to emphasize the impact of information sharing among agents, we contribute the following environments (adapted from [18]):

- **HearSee (HS):** Two heterogeneous agents cover a single landmark in a 2D map. The “Hear” agent observes the absolute position of the landmark, but it does not have access to its own position in the environment. The “See” agent observes the position and velocities of both agents, yet does not have access to the position of the landmark.
- **SpreadXY-2 (SXY-2):** Two heterogeneous agents cover two designated landmarks in a 2D map while avoiding collisions. In this scenario, one of the agents has access to the X-axis position and velocity of both agents, while the other agent has access to the Y-axis position and velocity of both agents. Both agents observe the landmarks’ absolute position;
- **SpreadXY-4 (SXY-4):** Similar to the scenario above but with two teams of two agents;
- **SpreadBlindfold (SBF):** Three agents cover three designated landmarks in a 2D map while avoiding collisions. Each agent’s observation only includes its own position and velocity and the absolute position of all landmarks;

In addition to the proposed environments, we evaluate our approach in the standard **SpeakerListener (SL)** environment from [18], as well as the **Level-Based Foraging** (Foraging-2s-15x15-2p-2f-coop-v2) (LBF) environment [17], which we modified to comprise the absolute positions of the agents. For some scenarios in standard benchmarks, such as the Multi-Agent Particle Environment [18], or Level-Based Foraging [17], we observed no advantage in allowing observation sharing between the agents even without considering communication failures (more details in Appendix B.1). Thus, we did not consider such environments in this work. For a complete description of the scenarios, as well as additional details regarding the choice of the environments used, we refer to Appendix B.1.

Finally, we consider H-POMDPs with communication matrices C such that each agent can always access its own observation, i.e., $p_{i,i} = 1$, and C is symmetric, i.e., $p_{i,j} = p_{j,i}$. To simplify the exposition, we use the same $p = p_{i,j}$ for all pairs of agents i, j . Therefore, we use p to unambiguously denote the communication level of a given H-POMDP. Nevertheless, for completeness, we perform a comparative study between different sampling schemes for C in Section 4.3.2, highlighting the robustness of MARO under different communication settings.

4.2. Baselines and experimental methodology

We compare MARO against the following baselines, which do not make use of a predictive model and perform constant imputation of missing observations:

- **Observation (Obs.):** Agents only have access to their own observations and are unable to communicate with other agents during execution. Corresponds to standard MARL algorithms designed for decentralized execution.
- **Masked Joint-Observation (Masked j. obs.):** During the centralized training phase, the RL controllers receive as input the concatenation of the observations of all agents. At execution-time, missing observations are replaced with a vector of zeros.
- **Message-Dropout (MD):** During the centralized training phase, the RL controllers receive as input the concatenation of the observations of all agents, but a dropout-based mechanism randomly drops some of the observations (i.e., replaces them with

Table 1

Performance of different value-based algorithms across all environments considered in this work. We report the 95% bootstrapped confidence interval alongside the corresponding scalar mean episodic returns. We perform 3 training runs for each experimental setting and 100 evaluation rollouts for each training run.

Env.	IQL					QMIX				
	Obs.	Masked j. obs.	MD	MD w/ masks	MARO	Obs.	Masked j. obs.	MD	MD w/ masks	MARO
SL	-40.0 (-0.4,+0.4)	-45.3 (-1.2,+1.9)	-25.4 (-0.6,+1.1)	-25.5 (-0.6,+1.1)	-25.3 (-0.6,+1.0)	-24.9 (-0.1,+0.0)	-40.5 (-0.8,+0.8)	-25.2 (-0.6,+1.1)	-25.2 (-0.6,+1.1)	-25.1 (-0.6,+1.2)
HS	-114.5 (-2.0,+1.6)	-64.0 (-2.1,+2.5)	-34.8 (-1.6,+1.7)	-34.1 (-1.3,+2.5)	-29.6 (-1.0,+0.7)	-62.2 (-1.9,+1.4)	-67.4 (-4.6,+3.0)	-29.2 (-1.3,+0.9)	-29.1 (-0.9,+0.8)	-28.8 (-1.2,+1.9)
SXY-2	-199.6 (-0.9,+0.9)	-202.9 (-2.3,+3.7)	-165.2 (-0.5,+0.7)	-160.7 (-1.7,+1.6)	-148.0 (-0.4,+0.5)	-177.8 (-7.6,+4.1)	-201.2 (-2.3,+2.3)	-157.2 (-1.4,+0.7)	-154.5 (-0.5,+1.0)	-145.7 (-0.9,+0.5)
SXY-4	-1225.5 (-4.2,+4.9)	-1161.2 (-7.6,+9.4)	-1157.0 (-1.2,+1.0)	-1164.5 (-10.8,+13.3)	-988.3 (-21.7,+37.4)	-1132.6 (-6.6,+5.9)	-1146.4 (-12.7,+22.1)	-1024.6 (-39.5,+54.9)	-1014.0 (-40.4,+40.6)	-850.0 (-22.5,+17.0)
SBF	-425.1 (-1.1,+1.4)	-415.5 (-7.5,+4.1)	-401.2 (-6.5,+8.5)	-400.5 (-5.5,+8.2)	-399.3 (-5.2,+6.4)	-416.1 (-10.0,+7.7)	-407.3 (-1.9,+1.5)	-401.4 (-4.9,+3.5)	-398.3 (-3.0,+2.3)	-382.3 (-5.2,+5.7)
LBF	0.38 (-0.03,+0.01)	0.19 (-0.02,+0.01)	0.53 (-0.03,+0.02)	0.52 (-0.02,+0.02)	0.35 (-0.01,+0.02)	0.55 (-0.01,+0.0)	0.25 (-0.05,+0.03)	0.58 (-0.01,+0.02)	0.59 (-0.02,+0.02)	0.44 (-0.02,+0.02)

Table 2

Performance of different actor-critic-based algorithms across all environments considered in this work. We report the 95% bootstrapped confidence interval alongside the corresponding scalar mean episodic returns. We perform 3 training runs for each experimental setting and 100 evaluation rollouts for each training run.

Env.	IPPO					MAPPO				
	Obs.	Masked j. obs.	MD	MD w/ masks	MARO	Obs.	Masked j. obs.	MD	MD w/ masks	MARO
SL	-33.3 (-11.6,+5.9)	-39.5 (-0.8,+0.7)	-45.2 (-5.0,+5.0)	-47.0 (-3.2,+4.0)	-25.2 (-0.1,+0.1)	-59.6 (-0.5,+0.6)	-39.3 (-1.2,+1.0)	-28.2 (-0.3,+0.3)	-27.5 (-0.4,+0.5)	-25.2 (-0.1,+0.1)
HS	-114.1 (-37.7,+27.7)	-81.8 (-5.8,+7.0)	-102.9 (-20.9,+22.5)	-101.9 (-19.4,+20.1)	-31.4 (-1.4,+1.2)	-70.5 (-18.3,+10.1)	-82.2 (-6.4,+3.3)	-32.4 (-0.0,+0.0)	-30.9 (-3.5,+2.6)	-31.4 (-1.4,+1.2)
SXY-2	-235.6 (-0.6,+0.6)	-214.8 (-5.4,+4.6)	-184.9 (-5.8,+3.6)	-175.9 (-3.0,+2.7)	-160.7 (-1.3,+1.0)	-212.6 (-13.7,+24.5)	-221.5 (-2.3,+3.2)	-181.1 (-3.9,+2.2)	-163.5 (-2.3,+2.7)	-161.2 (-0.9,+0.8)
SXY-4	-1133.2 (-7.1,+8.4)	-1162.1 (-33.8,+33.8)	-1124.7 (-27.6,+16.9)	-1177.9 (-29.4,+38.5)	-920.6 (-50.1,+92.7)	-1116.9 (-43.2,+79.0)	-1196.5 (-29.8,+20.3)	-1112.1 (-28.9,+26.4)	-1149.7 (-12.5,+16.3)	-827.4 (-7.8,+5.8)
SBF	-436.3 (-74.5,+38.4)	-403.1 (-2.1,+2.7)	-446.6 (-5.6,+6.4)	-472.7 (-9.7,+12.5)	-401.7 (-0.5,+0.6)	-420.3 (-0.4,+0.4)	-403.3 (-0.8,+1.2)	-407.3 (-1.8,+2.8)	-412.5 (-1.9,+3.3)	-399.9 (-1.2,+0.9)
LBF	0.31 (-0.0,+0.0)	0.3 (-0.01,+0.01)	0.03 (-0.02,+0.05)	0.01 (-0.01,+0.02)	0.37 (-0.01,+0.02)	0.36 (-0.0,+0.0)	0.31 (-0.02,+0.03)	0.02 (-0.01,+0.02)	0.02 (-0.02,+0.03)	0.38 (-0.03,+0.04)

a vector of zeros) according to $p \sim \mathcal{U}(0, 1)$. At execution-time, missing observations are replaced with a vector of zeros. This baseline is adapted from [19].

- **Message-Dropout w/ masks (MD w/ masks):** This baseline is similar to the MD baseline, but additionally appends to the input of the RL controllers a set of binary flags encoding whether the observations of the agents are missing or not. The masks give additional context to the RL agent regarding the validity of the entries in the vector of observations.

All baselines above can be used in the context of hybrid execution. Additionally, we consider an **Oracle** baseline under which all agents have access to the observations of all agents both during training and execution. Such oracle baseline corresponds to standard MARL algorithms designed for centralized execution, however, it is unable to perform when communication fails. We use the Oracle baseline to better contextualize the performance of the methods developed for hybrid execution against an optimal setting featuring no communication failures.

We employ the same RL controller networks across all evaluations. The RL networks include recurrent layers to mitigate the effects of partial observability. We consider four different MARL algorithms: IQL, QMIX, IPPO, and MAPPO. We perform 3 training runs for each experimental setting and 100 evaluation rollouts for each training run. We report, both in tables and plots, the 95% bootstrapped confidence interval alongside the corresponding scalar mean value. We assume that $p = 1$ at $t = 0$ for all algorithms. The algorithms are evaluated for $p \sim \mathcal{U}(0, 1)$ whenever the communication level is not explicitly referred, or for a given fixed communication level p when explicitly specified. The Oracle baseline is always evaluated with $p = 1$. We refer to Appendix B.2 for a complete description of the experimental methodology, hyperparameters, and the code used for this work.

4.3. Results

We present the main evaluation results in Tables 1 and 2 for the value-based and actor critic-based algorithms respectively. For each environment, RL algorithm and method, we present the values of the accumulated rewards obtained, for $p \sim \mathcal{U}(0, 1)$. The values that are not significantly different than the highest are presented in bold. The results show that MARO is the best-performing method overall. In particular, out of the 24 algorithm-environment combinations considered, MARO performed equal to or better than all

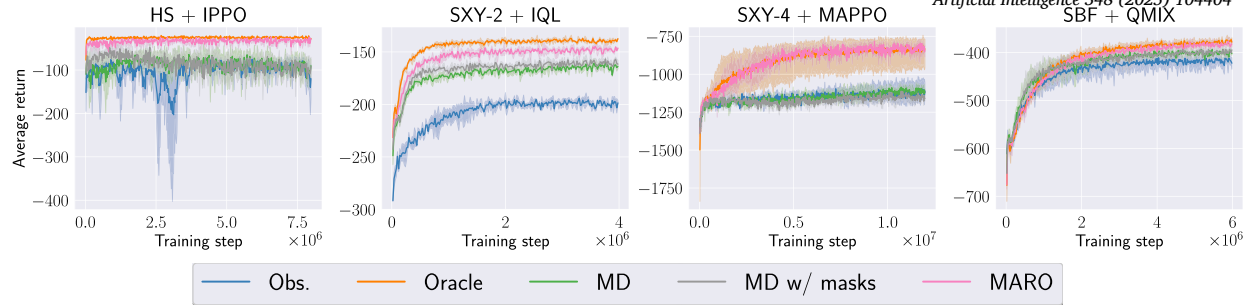


Fig. 3. Training curves for the methods with $p \sim \mathcal{U}(0, 1)$, considering different algorithms and environments. In the curves, we report the 95% bootstrapped confidence interval alongside the corresponding mean episodic returns. We perform 3 training runs for each setting and 100 evaluation rollouts for each training run.

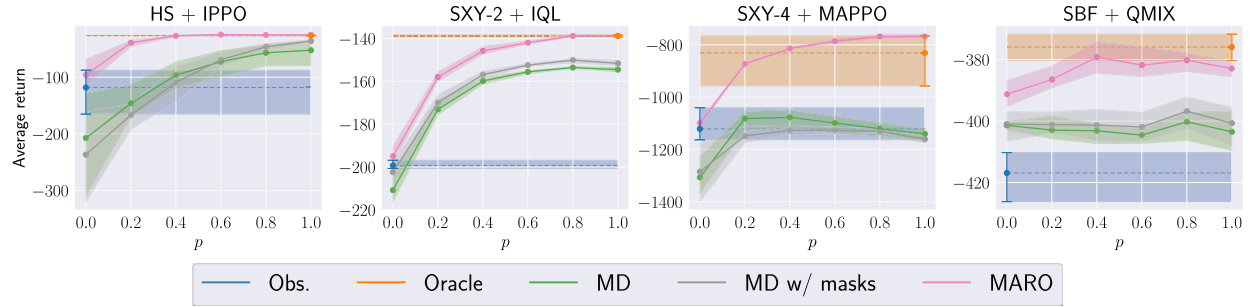


Fig. 4. Performance of the methods during execution for different communication levels p , considering different algorithms and environments. We present the 95% bootstrapped confidence interval alongside the corresponding mean episodic returns. We perform 3 training runs for each setting and 100 evaluation rollouts for each training run.

baselines for 22 of them (we further dissect the two settings for which MARO did not perform the best in Section 4.3.1). Overall, MARO is able to exploit the information provided by the other agents, in contrast with the fully decentralized approaches (Obs.). The obtained results show that the use of a predictive model of other agents' observations, as in MARO, allows for improved performance.

Additionally, we recall that the RL controllers of MARO are trained in a fully centralized manner, i.e., without considering communication failures at training time. Thus, an interesting observation is that MARO can be seen as a method that provides robustness to centralized execution methods when performing tasks in settings with potential faulty communication, despite never being trained to execute in such conditions. This is clear when comparing the performance of the two methods that consider a centralized training of the RL controllers (without considering communication failures during training), i.e., Masked j. obs. and MARO. As can be seen in Table 1 and Table 2, MARO's predictive model allows for zero-shot multi-agent execution with respect to communication failures, significantly outperforming the Masked j. obs baseline.

In Fig. 3, we highlight the training curves of MARO and the MD baselines, for $p \sim \mathcal{U}(0, 1)$ under some experimental configurations. We display the training curves for all methods, RL algorithms and environments in Appendix B.3. As can be seen, MARO achieves higher returns throughout training as compared to the other baselines. Additionally, MARO attains a performance similar to that of the Oracle baseline. In Fig. 4, we display the episodic returns of MARO and the MD baselines for different communication levels at execution time for some experimental configurations (more in Appendix B.3). As can be seen, MARO outperforms the MD baselines across the different communication levels. For the displayed environment-algorithm configurations, MARO always performs better or equal to the decentralized (Obs.) baseline, even when $p = 0$. Contrarily, this is not always the case for the MD baselines, as can be seen, for example, for the SXY4 + MAPPO configuration. Moreover, the performance of MARO improves as the level of communication in the environment increases, showing that our approach is able to efficiently make use of all provided information, contrary to the standard fully-decentralized approaches (Obs.).

As the previous results point out, the use of a predictive model to estimate missing agents' observations, the core component of MARO and the main distinguishing feature over the remainder baselines, is key for the improved performance of MARO. MARO outperforms the recurrent dropout-based baselines, irrespective of whether dropout is incorporated during training (MD baseline) and/or additional context is given to the RL controllers regarding the validity of the entries in the joint-observation vector (MD w/ masks baseline). While previous results attest that the predictions of the predictive model are useful for control, we can also directly visualize the quality of the predictions themselves. In Fig. 5, we show the predicted trajectories of all agents from the perspective of each of the agents. As seen, the predicted trajectories are close to the real trajectories of the agents (more in Appendix B.3.3). The predictive model is thus able to perform accurate agent modeling with faulty communication, providing an interpretable insight into the decision-making process of the agents.

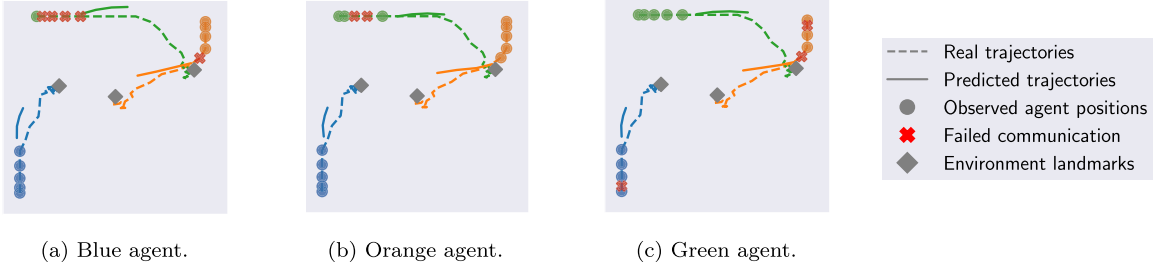


Fig. 5. Estimation of the trajectories of the agents made by the predictive model at $t = 4$ (SBF, QMIX). The plots are computed, from the perspective of each agent, by computing the estimated trajectories of all agents for the next 4 timesteps. The predictions are computed in a fully auto-regressive manner.

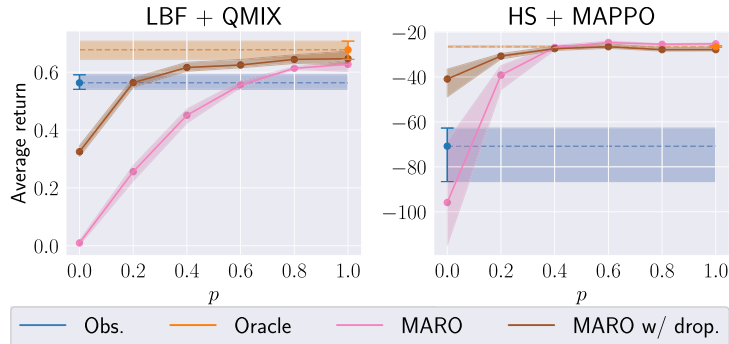


Fig. 6. Performance of MARO and MARO without dropout during execution for different communication levels p , considering different algorithms and environments. We present the 95% bootstrapped confidence interval alongside the corresponding mean episodic returns. We perform 3 training runs for each experimental setting and 100 evaluation rollouts for each training run.

Table 3

Performance of MARO without dropout during execution with $p \sim \mathcal{U}(0, 1)$, considering different algorithms and environments. We present the 95% bootstrapped confidence interval alongside the corresponding mean episodic returns. We perform 3 training runs and 100 evaluation rollouts for each training run.

Env.	Algo.	MARO w/ drop.
LBF	IQL	0.52 (-0.01, +0.01)
LBF	QMIX	0.60 (-0.01, +0.02)
HS	MAPPO	-28.7 (-1.4, +1.2)
SXY-2	MAPPO	-159.6 (-0.3, +0.3)

In the next sections, we: (i) assess the impact of considering communication failures at training time, investigating the experimental settings for which MARO was not the best method, in Section 4.3.1; and (ii) evaluate the performance of MARO under different communication protocols, in Section 4.3.2.

4.3.1. On the impact of communication dropout at training time

We now focus our attention on the two settings from Tables 1 and 2 under which the MD baselines outperformed MARO. In Fig. 6, we display the performance of MARO for different communication levels under the LBF + QMIX setting, as well as the HS + MAPPO experimental configuration. As can be seen, the performance of MARO deteriorates for low levels of communication, likely because the RL controllers never had to rely almost entirely on estimations from the predictive model during training. Therefore, we now investigate the impact of considering communication failures also during the training of MARO. To do so, we consider MARO w/ drop., an alternate version of MARO under which a dropout-based mechanism randomly drops some of the observations of the agents during training according to $p \sim \mathcal{U}(0, 1)$. The dropped observations are replaced with predictions from the predictive model. We emphasize that it is fair to compare the performance of MARO w/ drop. against the other baselines, as the MD and MD w/ masks baselines already consider a dropout-based training scheme.

As displayed in Fig. 6, it is clear that the inclusion of a dropout-based training mechanism to MARO greatly contributed to improve the performance of the method, especially for the settings featuring a low degree of communication (low values of p in the plot). In Table 3, we display the mean episodic returns for MARO under four experimental configurations. As can be seen, when comparing with the values obtained by MARO in Tables 1 and 2, the performance of MARO further improved for the aforementioned experimental

Table 4

Performance of the methods during execution for different communication protocols, considering different algorithms and environments. We present the 95% bootstrapped confidence interval alongside the corresponding mean episodic returns. We perform 3 training runs for each experimental setting and 100 evaluation rollouts for each training run.

Env.	Algo.	$p_{\text{asymmetric}}$			p_{dynamic}				
		Masked j. obs.	MD	MD w/ masks	MARO	Masked j. obs.	MD	MD w/ masks	MARO
SXY-2	IQL	-200.2 (-0.5,+0.4)	-164.1 (-1.1,+0.7)	-160.5 (-0.8,+0.6)	-149.4 (-0.2,+0.3)	-196.7 (-2.3,+2.2)	-161.2 (-0.4,+0.3)	-157.6 (-0.8,+0.8)	-145.3 (-1.0,+1.5)
	SBF	-407.3 (-6.8,+6.6)	-403.7 (-8.4,+4.4)	-401.0 (-6.6,+5.0)	-380.8 (-2.1,+3.3)	-404.6 (-2.7,+2.0)	-402.7 (-6.7,+3.5)	-398.6 (-4.2,+4.5)	-381.9 (-5.0,+5.6)
LBF	IPPO	0.30 (-0.01,+0.0)	0.03 (-0.03,+0.05)	0.01 (-0.01,+0.01)	0.36 (-0.01,+0.01)	0.31 (-0.02,+0.01)	0.03 (-0.03,+0.06)	0.02 (-0.01,+0.02)	0.40 (-0.03,+0.03)
	SXY-4	-1066.9 (-23.2,+28.7)	-1128.1 (-26.2,+20.1)	-1160.7 (-12.0,+13.1)	-823.9 (-1.9,+1.8)	-1068.3 (-2.7,+4.4)	-1101.7 (-32.2,+23.5)	-1136.7 (-13.5,+16.8)	-813.0 (-3.4,+2.9)

settings by considering dropout at training time. In particular, we highlight that, for the two experimental settings under which the MD baselines outperformed MARO, MARO w/ drop. is now able to equal the performance of the best-performing method.

The results above show that the inclusion of a dropout-based mechanism can impact the performance of the algorithm for hybrid execution. We display the experimental results obtained for MARO w/ drop. for all environments and RL algorithms in Appendix B.3. We note that, according to our results, the improvement of MARO over MARO w/ drop. was not consistent over all tested algorithm-environment configurations. In fact, for some experimental settings, MARO outperformed MARO w/ drop. Therefore, we decided to treat the use of the dropout-based mechanism in the training of MARO as an hyperparameter that should be tuned according to each experimental scenario. Nevertheless, we highlight that MARO and MARO w/ drop. were the best-performing methods overall.

4.3.2. On the impact of the sampling scheme of the communication matrix at execution time

Finally, in order to better understand MARO's performance under different communication protocols, we evaluate different sampling schemes of the communication matrix: (i) our default setting, p_{default} , under which $p_{i,j} = p_{j,i} = p$ with $p \sim \mathcal{U}(0, 1)$, sampled at the beginning of each episode; (ii) $p_{\text{asymmetric}}$, featuring communication matrices C such that $p_{i,j} \neq p_{j,i} \sim \mathcal{U}(0, 1)$, sampled at the beginning of each episode; and (iii) p_{dynamic} , similar to (ii) but with C 's sampled every 5 time steps. We present the results in Table 4 for a subset of all RL algorithm-environment combinations. As can be seen, MARO continues to perform equal to or better than the remainder baselines, independently of the sampling scheme. We display the complete results in Appendix B.3; across all results, either MARO or MARO w/ drop. performed equal to or better than all other baselines.

5. Related work

In this section, we connect our work with other lines of research, discussing the similarities and differences between our approach and previous works in the field. We discuss only the most relevant works and provide an extended discussion of related work in Appendix A.

Closely related to our work are papers that address the problem of partial observability in MARL. As an example, [20] propose a decentralized MARL algorithm that uses RNNs to improve the agents' observability. The work [21] uses an RNN to compress the agents' histories, helping to improve agents' observability. The commonly used paradigm of centralized training with decentralized execution also contributes to alleviating partial observability at training time [5–7,22]. Other lines of research investigate communication techniques for MARL [10], focusing on how [23,24], when [25,26], and what [7] to communicate to foster cooperation. Previous works focused on the sharing of (encoded) local observations and actions among agents [7] in a proxy-like manner [27]. Others consider learning robust communication protocols under missing information. Some approaches learn mechanisms that improve communication efficiency by either limiting the variance of exchanged messages [28] or temporally smoothing information shared between agents [29]. The work [19] proposes message-dropout, which aims at making learning robust against communication errors. Message-dropout drops the messages received from other agents independently at random during training before inputting them into the RL algorithm. In a similar fashion to message dropout, [30] propose a recurrent actor-critic algorithm for handling multi-agent coordination under partial observability with limited communication, showing that recurrency successfully contributes to robust performance under communication failures.

In contrast, we assume that agents have no control over when and with whom to communicate. Hence, they should robustly perform under any type of communication policy/level at execution time. Also, we do not learn the content of the messages and consider a rather passive communication setting in which agents share local observations and actions. For this reason, we did not include the works [28,29] as baselines since the comparison between methods would not be meaningful. Instead, following [19,30], we use message-dropout with recurrent learners as a baseline. Finally, none of the aforementioned works proposed the use of predictive models to account for missing information at execution time as we do in our work.

Other lines of research are also relevant to our work. As opposed to agent/opponent modeling [31–33], we aim at learning policies for multiple agents concurrently. In contrast to multi-agent trajectory prediction [34–36,16], we consider a rather broader setting in which agents' observations can correspond to any type of information collected by the agents and use the predictive model with

the objective of being robust to missing information. Finally, while our method can be categorized as a model-based MARL method [37–39], as opposed to previous works which are mainly focused on increasing sample efficiency, we use the predictive model to estimate missing observations.

6. Conclusion

In this work, we study *hybrid execution* in MARL, a paradigm in which agents act under any communication level at execution time, while exploiting information-sharing among the agents. To allow for hybrid execution we propose MARO, a novel approach that consists of an autoregressive predictive model to estimate missing observations. We show that MARO’s predictive model allows for successful agent trajectory modeling across different communication levels, successfully exploiting available shared information and contributing to improved performance over the remainder baselines.

Future work We envision that the paradigm of centralized training with hybrid execution can intersect with many other research directions within the field of MARL. First, an interesting research direction is to investigate the performance of MARO, as well as the baselines, in scenarios comprising a higher number of agents. Second, there may be scenarios in which observation-sharing among the agents can be prohibitive due to limited bandwidth or privacy concerns; thus, under such scenarios, it may be interesting to combine the ideas herein presented with, for example, the learning of low-dimensional representations of the agents’ observations. Third, an interesting research idea is to study MARO under learned communication protocols such as in [7]; this may allow agents to achieve improved performance as the agents are able to learn useful messages to communicate with other agents. Finally, other future work could comprise studying other neural network architectures, such as graph neural networks, for better trajectory prediction, or hybrid execution under noisy/corrupted communication channels.

CRediT authorship contribution statement

Pedro P. Santos: Writing – review & editing, Writing – original draft, Software, Methodology, Investigation, Conceptualization. **Diogo S. Carvalho:** Writing – review & editing, Writing – original draft, Software, Methodology, Investigation, Conceptualization. **Miguel Vasco:** Writing – review & editing, Writing – original draft, Software, Methodology, Investigation, Conceptualization. **Alberto Sardinha:** Writing – review & editing, Supervision, Resources, Conceptualization. **Pedro A. Santos:** Supervision, Resources. **Ana Paiva:** Supervision, Resources. **Francisco S. Melo:** Writing – review & editing, Supervision, Resources, Conceptualization.

Declaration of competing interest

The authors declare the following financial interests/personal relationships which may be considered as potential competing interests: Pedro P. Santos reports financial support was provided by Fundação para a Ciência e a Tecnologia. Diogo S. Carvalho reports financial support was provided by Fundação para a Ciência e a Tecnologia. Miguel Vasco reports financial support was provided by Swedish Research Council. Miguel Vasco reports financial support was provided by Knut and Alice Wallenberg Foundation. Miguel Vasco reports financial support was provided by European Research Council. If there are other authors, they declare that they have no known competing financial interests or personal relationships that could have appeared to influence the work reported in this paper.

Acknowledgements

This work was supported by Portuguese national funds through the Portuguese Fundação para a Ciência e a Tecnologia (FCT) under projects UIDB/50021/2020 (INESC-ID multi-annual funding), PTDC/CCI-COM/5060/2021 (RELEvAENT), AI-PackBot LISBOA2030-FEDER-00854700 (project number 14935), and WSMART ROUTEs+ (2022.04180.PTDC). Pedro P. Santos acknowledges the Fundação para a Ciência e a Tecnologia (FCT) PhD grant 2021.04684.BD, and Diogo S. Carvalho the PhD grant 2020.05360.BD. This work has also been supported by the Swedish Research Council, Knut and Alice Wallenberg Foundation and the European Research Council (ERC-BIRD 884807). The authors also thank the lab managers at GAIPS for the support provided when running the computational experiments of this work.

Appendix A. Extended related work

In this section, we connect our work with other lines of research, discussing the similarities and differences between our study and previous works in the field. The discussion herein presented corresponds to an extended version of Sec. 5.

A.1. Partial observability in MARL

Closely related to our work are studies that address the problem of partial observability in MARL. As an example, [20] propose a decentralized MARL algorithm that uses RNNs to improve the agents’ observability. The work [21] uses an RNN to first compress the agents’ histories into embeddings that are posteriorly fed into deep Q-networks, helping to improve agents’ observability. The commonly used paradigm of centralized training with decentralized execution also contributes to alleviating partial observability

at train time [5–7,22]. Under such paradigm, the calculation of value functions or policy gradients can exploit the centralization of information, thus alleviating partial observability.

Another way to alleviate the problem of partial observability in MARL, especially at test time, is to consider communication between the agents. We review such setting in the following section.

A.1.1. Communication in MARL

Different lines of research focus their attention on the development of communication techniques for MARL [10], focusing on how the sharing of information between the agents can be used to improve the RL agents' learning. Early works addressed communication under partially observable cooperative MARL tasks: [40] shares the outputs of the hidden layers of a shared neural network among the agents; [7] explicitly learns the content of the messages transmitted between agents by following an end-to-end approach in which gradients are back-propagated through the communication variables. Recent works in the field study how [23,24], when [25,26], and what [7] should be communicated among the agents in order to foster cooperation.

Similarly to our work, previous studies focused on the sharing of (encoded) local observations and actions among agents [7] in a proxy-like manner [27]. However, as opposed to previous works, we assume that agents have no control over when and with whom to communicate and, instead, should robustly perform under any type of communication policy. We also emphasize that we are not focused on learning the content of the messages being communicated (as in [7]), focusing our attention on a rather “passive” communication setting by considering the sharing of local observations and actions among the agents. Other works focus on learning how to combine received information with local information before feeding it into the RL model [41,27]. In our work, we concatenate received information alongside local information. However, the methods developed by previous studies, which can be seen as orthogonal contributions in comparison to our work, can be readily incorporated into our method.

Finally, some works consider learning robust communication protocols under failing/missing information. Previous studies learn mechanisms that improve communication efficiency by either limiting the variance of exchanged messages [28], or temporally smoothing information shared between agents [29]. Due to the decreased variability of the messages exchanged throughout timesteps, such methods achieve improved robustness against transmission loss. However, since in this work we are not focusing our attention on methods that learn the contents of the messages being exchanged, we did not use the aforementioned methods as baselines in our work as the comparison between methods would be deemed inappropriate. The work [19] proposes a learning technique for MARL called message-dropout, which aims at: (i) effectively handling the increased input dimension in MARL with communication; and (ii) making learning robust against communication errors in the execution phase. Message-dropout drops the messages received from other agents independently at random during training before inputting them into the RL algorithm. In a similar fashion to message dropout, [30] proposes a recurrent actor-critic algorithm for handling multi-agent coordination under partial observability with limited communication, showing that recurrence successfully contributes to robust performance when communication fails. Following [19,30], we use message-dropout with recurrent learners as a baseline in our work.

We refer to [10] for an extensive discussion of the different works that propose communication protocols for MARL.

A.2. Modeling other agents

In contexts where a single agent learns in an environment where other agents are also present, some works have explored ways to model information about the other agents, such as their actions and observations, based on local information available to the learning agent. The work of [31] uses a recurrent neural network to predict the other agents' actions and observations in order to make better action selections in a centralized training with decentralized execution setting. At execution time, the agent then uses its learned model to make explicit predictions about other agents' observations and actions. [32] does similarly in a latent space. The work of [33] uses, instead, the other agents' observations to predict their actions, which assumes centralization will be available at execution time.

Contrarily to the mentioned settings, in ours, we aim at learning policies for multiple agents. To that end, we use a model of the agents' observations and actions to make predictions about other agents and improve their performance in cooperative tasks.

A.3. Model-based MARL

Recently, different works addressed model-based MARL, being mostly focused on improving the sample efficiency of MARL methods by leveraging the knowledge of the learned environment dynamics in policy optimization [42,37]. Closely related to our work are studies that propose model-based approaches to MARL while considering communication among the agents. As an example, [38] proposes a communication protocol that encodes into the message an agent's imagined trajectory computed by performing rollouts using an opponent model and a dynamics function.

As opposed to previous works, in our work we focus our attention on the study of methods that allow for robust execution under different communication degrees. While our method can be categorized as a model-based MARL method that implicitly models both the dynamics function as well as the other agents' policies, we use it with a rather different objective than the aforementioned articles.

We refer to [39] for an extensive discussion of model-based approaches to MARL.

A.4. Multi-agent trajectory prediction

There exists a number of works that address trajectory prediction under multi-agent settings using sequence models [34–36,16]. As an example, [34] uses an RNN to learn and predict the trajectory of pedestrians. The work [36] proposes an uncertainty-aware

Table B.5

Mean episodic returns for the SimpleSpread-v0 environment ($p \sim \mathcal{U}(0, 1)$). Higher is better.

Algorithm	SimpleSpread-v0	
	Obs.	Oracle
IQL	-393.9 (-4.5,+7.8)	-384.8 (-7.4,+3.8)
QMIX	-380.2 (-7.0,+6.8)	-373.8 (-4.5,+4.5)
IPPO	-400.9 (-2.9,+1.9)	-404.8 (-4.2,+3.6)
MAPPO	-401.8 (-1.2,+1.4)	-404.8 (-4.2,+3.6)

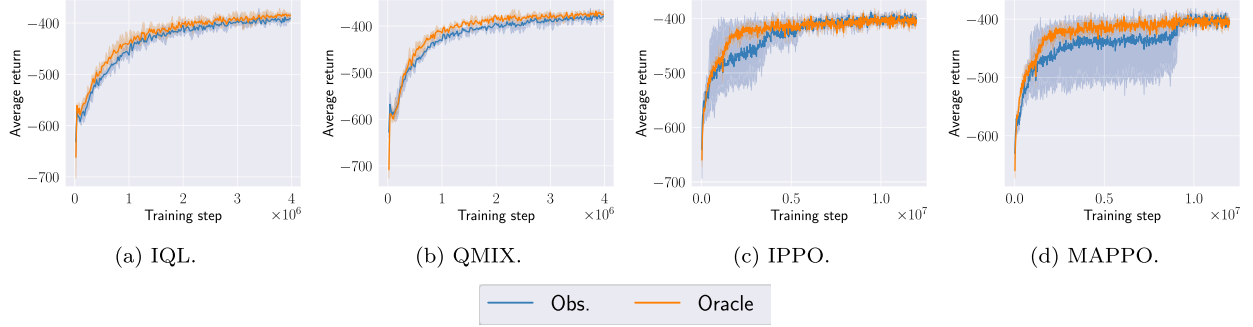


Fig. B.8. (SimpleSpread-v0) Mean episodic returns for $p \sim \mathcal{U}(0, 1)$ during training.

multi-modal deep learning model to predict multiple future trajectories of basketball players. In [16] is proposed a method based on graph neural networks and bi-directional RNNs to predict unobserved parts of football players' trajectories.

Our work resembles some similarities with the aforementioned studies since our predictive method MARO solves a similar problem to that of the aforementioned works if we consider that the observations correspond to agents' coordinates. However, in our study, we consider a rather broader setting in which agents' observations can correspond to any type of information collected by the agents. Importantly, we focus our attention on control settings whereas the previous works only deal with predictive settings. Also, we use the predictive model with the objective of being robust to missing information during agency. Nevertheless, we note that our method MARO can possibly benefit from techniques proposed by the aforementioned works.

Appendix B. Experimental evaluation

In this section, we present supplementary materials for Sec. 4. In Appendix B.1, we provide additional results to support the choice of environments used in this work and describe the proposed MARL scenarios in detail. In Appendix B.2, we describe our experimental methodology. Finally, we present our complete set of experimental results in Appendix B.3.

B.1. MARL scenarios

B.1.1. On the selection of the MARL scenarios

As described in the main text, in this work we are focused on developing methods for hybrid execution, i.e., methods that aim to successfully perform tasks under any degree of centralization. Implicit to our study is the idea that observation-sharing between the agents provides additional information that allows each agent to make better informed choices, thus leading to a better overall performance in comparison to fully decentralized approaches. As observed, however, this is not always the case for environments from standard benchmarks.

To illustrate the aforementioned, we compare the performance of the Obs. baseline (fully decentralized) and the Oracle baseline (fully centralized, without considering communication failures) under three different environments. In Table B.5 and Fig. B.8, we display the performance values for the standard SimpleSpread-v0 environment from the Multi-Agent Particle Environment [18]. As can be seen, the performance of the fully centralized approach (Oracle baseline) is similar to that of the fully decentralized approach (Obs. baseline). This happens because, for this environment, each agent gets to observe the relative positions of all other agents, as well as the positions of the landmarks, making the environment fully observable. Therefore, there are no gains in allowing information sharing between the agents. In Table B.6 and Fig. B.9, we display the experimental results for the Foraging-2s-15x15-2p-2f-coop-v2 from the Level-Based Foraging environment [18]. As can be seen, once again, the performances of the Obs. and Oracle baselines are very similar. This is the case because, in the Level-Based Foraging environment, the observation of each agent contains the relative positions of the agents/foods that are inside the field-of-view of the agent (as common to previous works, we consider the flag `grid_observation=False`). Since the relative positions of the agents/foods are considered, observation-sharing between the agents is of little help to improve agents' observability. Finally, in Table B.7 and Fig. B.10, we display the results obtained for the modified LBF environment, under which the agents' observations are modified to include the absolute position of the agents (more details in the

Table B.6

Mean episodic returns for the Foraging-2s-15x15-2p-2f-coop-v2 (Original) environment ($p \sim \mathcal{U}(0, 1)$). Higher is better.

Algorithm	Foraging-2s-15x15-2p-2f-coop-v2 (Original)	
	Obs.	Oracle
IQL	0.156 (-0.012,+0.012)	0.173 (-0.019,+0.021)
QMIX	0.308 (-0.039,+0.058)	0.335 (-0.033,+0.026)
IPPO	0.227 (-0.014,+0.019)	0.197 (-0.045,+0.046)
MAPPO	0.211 (-0.016,+0.014)	0.197 (-0.046,+0.046)

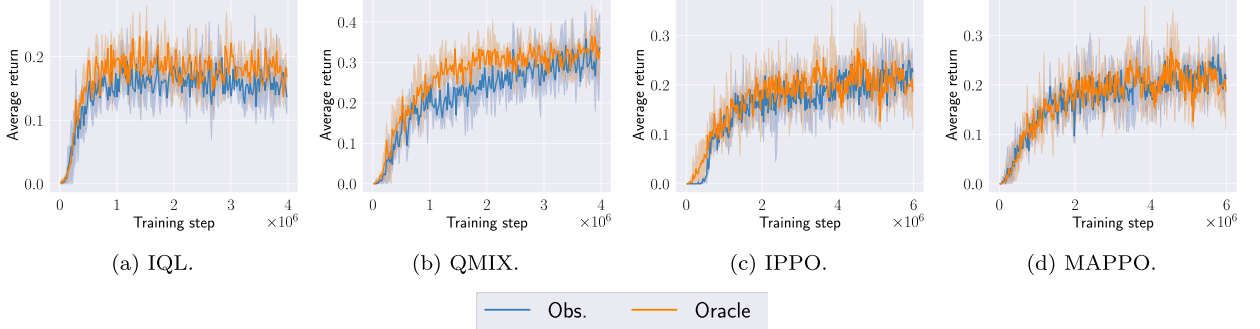


Fig. B.9. (Foraging-2s-15x15-2p-2f-coop-v2, Original) Mean episodic returns for $p \sim \mathcal{U}(0, 1)$ during training.

Table B.7

Mean episodic returns for the Foraging-2s-8x8-2p-2f-coop-v2 (Modified) environment ($p \sim \mathcal{U}(0, 1)$). Higher is better.

Algorithm	Foraging-2s-8x8-2p-2f-coop-v2 (Modified)	
	Obs.	Oracle
IQL	0.986 (-0.002,+0.001)	0.982 (-0.002,+0.002)
QMIX	0.978 (-0.007,+0.007)	0.971 (-0.012,+0.008)
IPPO	0.477 (-0.009,+0.004)	0.488 (-0.003,+0.004)
MAPPO	0.486 (-0.003,+0.004)	0.489 (-0.006,+0.008)

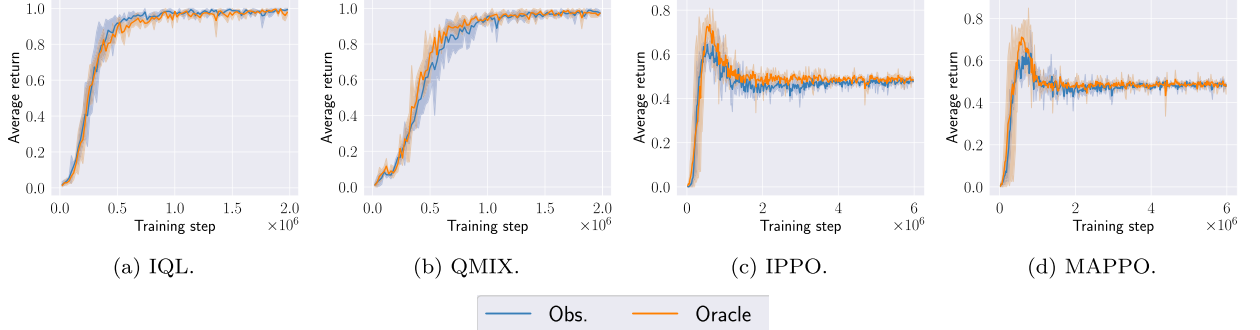


Fig. B.10. (Foraging-2s-8x8-2p-2f-coop-v2, Modified) Mean episodic returns for $p \sim \mathcal{U}(0, 1)$ during training.

next section). This environment is similar to the one considered in the main text but comprises a smaller grid size. As can be seen, the performance of both the Obs. and Oracle baselines are similar, across algorithms. We hypothesize that this is the case because, even though information sharing can help to improve agents' observability, the small grid size already contributes to alleviating the partial observability of the agents, thus making the task easier for the fully decentralized agents.

Given the results just presented, it is clear that we do not expect the cooperative team of agents to always benefit from information-sharing among the agents. Some environments are simply already fully observable from the perspective of each agent, while for others, observation-sharing may not contribute to improved performance. With that in mind, we decided to propose new multi-agent environments, described in the next section, which extend standard benchmarks in order to emphasize the negative impact of partial observability in MARL and, under which, the problem of hybrid execution is relevant. We believe the proposed environments are representative of a diverse number of multi-agent tasks.

B.1.2. Environments description

SimpleSpeakerListener (SL) Taken from the Multi-Agent Particle Environment [18].

HearSee (HS) The environment consists of two heterogeneous agents and a single landmark in a 2D map. At the start of each episode both the position of the agents and of the landmark is randomly generated. The goal of the agents is to cooperate in order for both of them to cover the landmark: agents are (globally) rewarded considering how far the closest agent is to each landmark (sum of the minimum distances). In this scenario, one of the agents (“Hear” agent) is provided with the absolute position of the landmark in its observation. However, it does not have access to its own position. The other agent (“See” agent) is able to access the position and velocities of both agents in its observation, yet does not have access to the position of the landmark. Only through communicating with the central proxy, can the agents have access to both their positions and the position of the landmark in order to complete the task.

SpreadXY-2 (SXY-2) The environment consists of two heterogeneous agents and two designated landmarks in a 2D map. At the start of each episode both the position of the agents and of the landmarks is randomly generated. The goal of the agents is to cover all the landmarks while avoiding collisions: agents are (globally) rewarded considering how far the closest agent is to each landmark (sum of the minimum distances) and are (locally) penalized if they collide with other agents. Differently from SSB, one of the agents has access to the X position and velocity of both agents, while the other agent has access to the Y position and velocity of both agents. Both agents observe as well the absolute position of all landmarks. Through communication with the central proxy, the agents can access the complete position and velocities of the other agents and cover the landmarks.

SpreadXY-4 (SXY-4) This environment is similar to *SpreadXY-2* but comprises two teams of two agents each. Within each team, one of the two agents has access to the X position and velocity of both agents, and the other has access to the Y position and velocity of both agents. Agents must cover the four landmarks while avoiding collisions between each other.

Spreadblindfold (SBF) The environment consists of three agents and three designated landmarks in a 2D map. At the start of each episode both the position of the agents and of the landmarks is randomly generated. The goal of the agents is to cover all the landmarks while avoiding collisions: agents are (globally) rewarded considering how far the closest agent is to each landmark (sum of the minimum distances) and are (locally) penalized if they collide with other agents. Differently from the original Simple Spread environment, the agent’s observation only includes the position and velocity of the agent itself and the relative position of all landmarks. Through communication with the central proxy, the agents can access the position and velocities of the other agents.

Foraging-2s-15x15-2p-2f-coop-v2 (LBF) Taken from the Level-Based Foraging environment [17], but with the agents’ observations modified to include the absolute position of the agents (if inside the field-of-view) instead of their relative positions. The positions of the food inside the field-of-view of each agent appear as relative positions in the observation vector as in the original environment. We consider parameter *grid observation=False*.

We refer to [18,17] for a visual depiction of the environments.

B.2. Experimental methodology and implementation

We employ the same RL controller networks across all evaluations. The RL networks include recurrent layers to mitigate the effects of partial observability. We consider four different MARL algorithms: IQL, QMIX, IPPO, and MAPPO. We perform 3 training runs for each experimental setting and 100 evaluation rollouts for each training run. We report, both in tables and plots, the 95% bootstrapped confidence interval alongside the corresponding scalar mean value. We assume that $p = 1$ at $t = 0$ for all algorithms. We display our training hyperparameters for the RL controllers and the predictive model in Tables B.8, B.9 and B.10. We developed our code in a Python environment using the EPyMARL framework [17] and PyTorch [43]. The computational code is available at <https://github.com/PPSantos/hybrid-marl>.

B.3. Experimental results

In this section, we display the complete experimental results. We present our main results in Appendix B.3.1. In Appendix B.3.2, we display the results of MARO under different communication protocols. In Appendix B.3.3, we display a set of figures that illustrates the predictions made by the predictive model.

B.3.1. Main experimental results

In this section, we present the complete experimental results of all approaches across all environments and algorithms. The results herein presented correspond to the full results for Sec. 4.3 of the main text. In this section, we display the mean episodic returns: (i) for a specific communication level p , when the communication level is explicitly referred; or (ii) for our default communication setting p_{default} , under which $p_{i,j} = p_{j,i} = p$ with $p \sim \mathcal{U}(0, 1)$, with communication matrices sampled at the beginning of each episode. The Oracle baseline is always evaluated with $p = 1$. (Table B.11, Figs. B.11–B.13, Table B.12, Figs. B.14–B.16, Table B.13, Figs. B.17–B.19, Table B.14, Figs. B.20–B.22, Table B.15, Figs. B.23–B.25, Table B.16, Figs. B.26–B.28.)

Table B.8

Hyperparameters for the RL controllers (MPE environments).

(a) IQL.		(b) QMIX.	
hidden dimension	256	hidden dimension	256
learning rate	0.0005	learning rate	0.0005
reward standardization	True	reward standardization	True
network type	GRU	network type	GRU
evaluation epsilon	0.0	evaluation epsilon	0.0
epsilon anneal	500,000	epsilon anneal	50,000
target update	200	target update	200
(c) IPPO.		(d) MAPPO.	
hidden dimension	256	hidden dimension	256
learning rate	0.0003	learning rate	0.0003
reward standardization	True	reward standardization	True
network type	GRU	network type	GRU
entropy coefficient	0.01	entropy coefficient	0.01
target update	200	target update	200
n-step	5	n-step	5

Table B.9

Hyperparameters for the RL controllers (LBF environments).

(a) IQL.		(b) QMIX.	
hidden dimension	256	hidden dimension	256
learning rate	0.0003	learning rate	0.0001
reward standardization	True	reward standardization	True
network type	GRU	network type	GRU
evaluation epsilon	0.0	evaluation epsilon	0.0
epsilon anneal	100,000	epsilon anneal	100,000
target update	200	target update	200
(c) IPPO.		(d) MAPPO.	
hidden dimension	256	hidden dimension	256
learning rate	0.0001	learning rate	0.0001
reward standardization	False	reward standardization	False
network type	GRU	network type	GRU
entropy coefficient	0.001	entropy coefficient	0.001
target update	200	target update	200
n-step	5	n-step	5

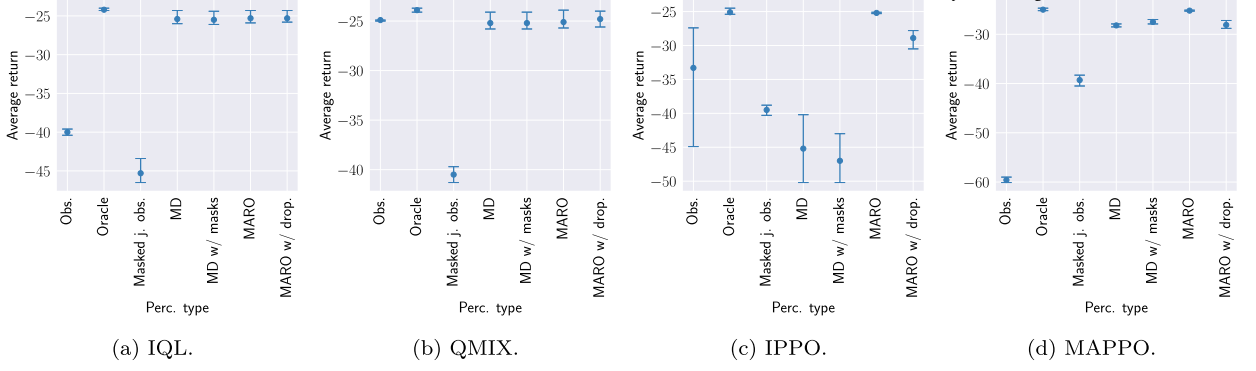
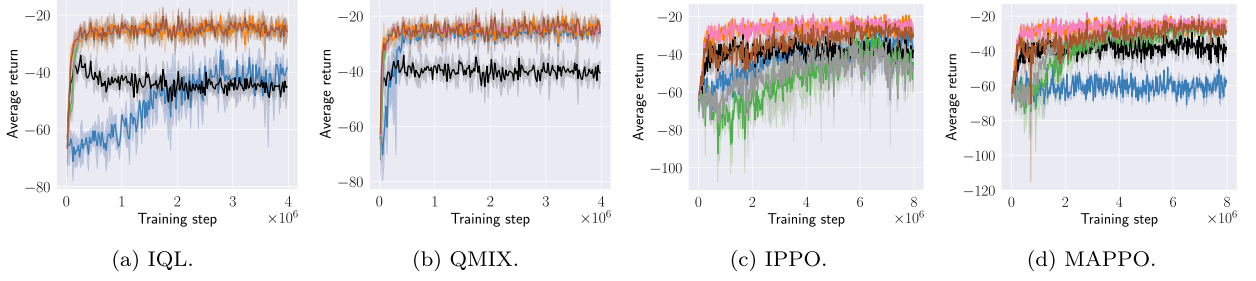
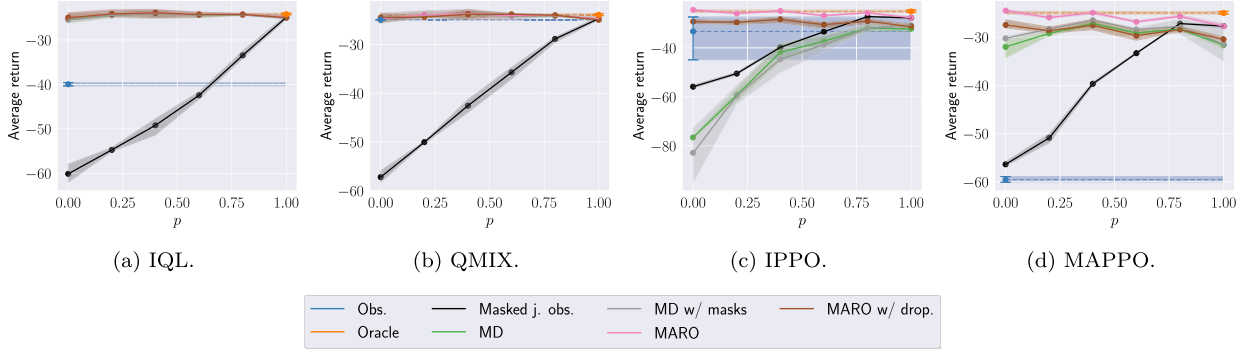
Table B.10

Hyperparameters for the predictive model across all environments and algorithms.

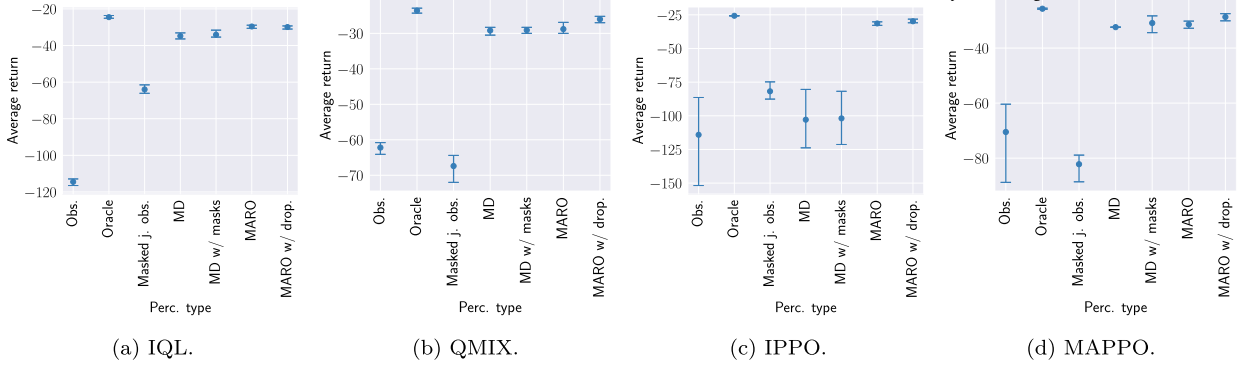
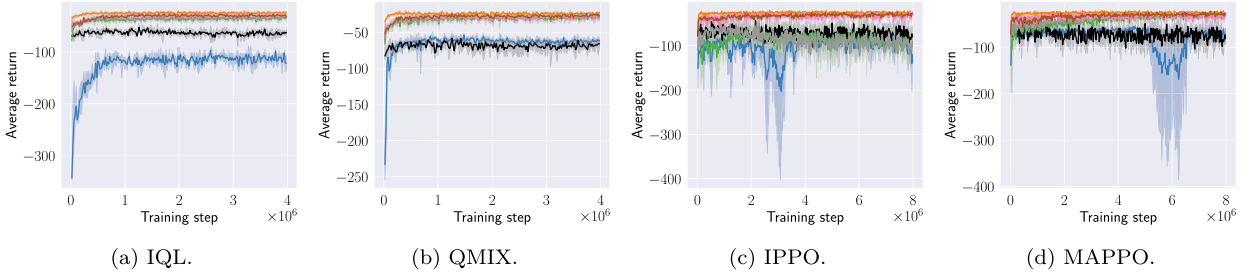
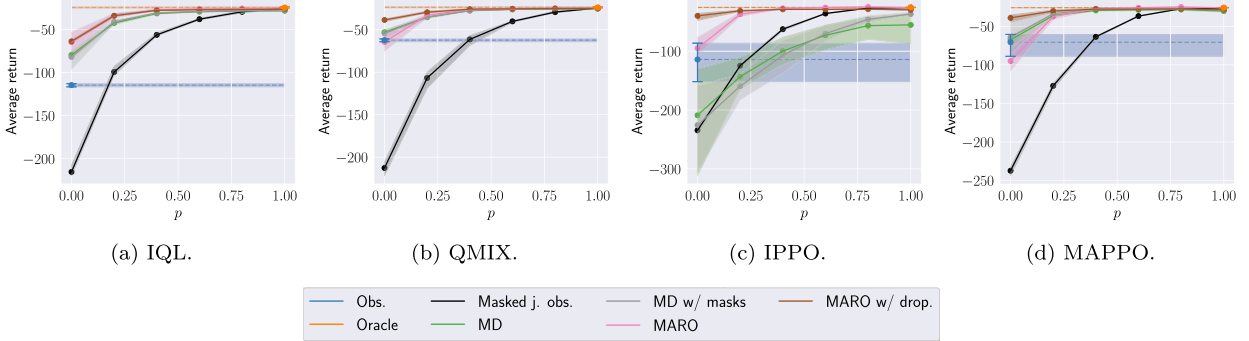
hidden dimension	128
learning rate	0.001
grad clip	1.0
buffer size	5 000
batch size	32

Table B.11(SpeakerListener) Mean episodic returns for p_{default} at execution time.

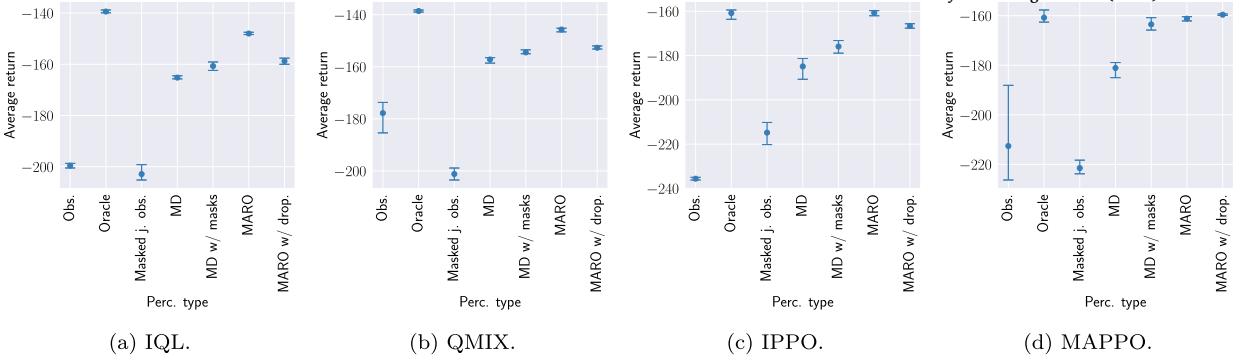
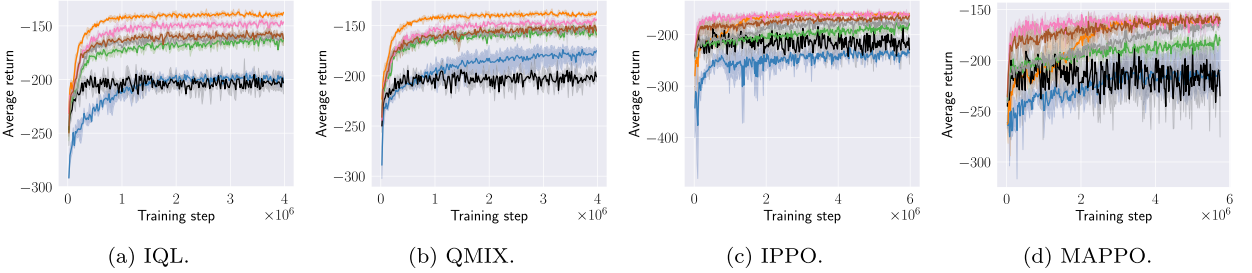
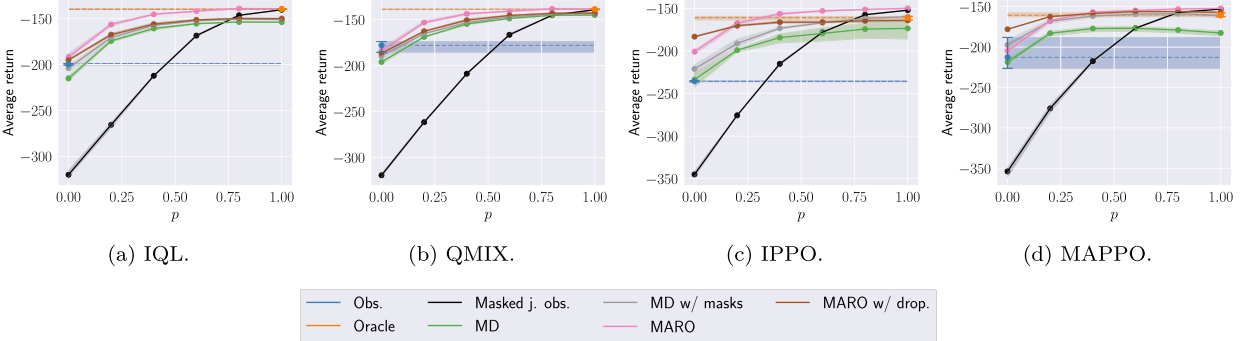
Algorithm	Obs.	Oracle	Masked j. obs.	SpeakerListener (p_{default})			
				MD	MD w/ masks	MARO	MARO w/ drop.
IQL	-40.0 (-0.4,+0.4)	-24.2 (-0.1,+0.2)	-45.3 (-1.2,+1.9)	-25.4 (-0.6,+1.1)	-25.5 (-0.6,+1.1)	-25.3 (-0.6,+1.0)	-25.3 (-0.5,+1.0)
	-24.9 (-0.1,+0.0)	-23.9 (-0.2,+0.2)	-40.5 (-0.8,+0.8)	-25.2 (-0.6,+1.1)	-25.2 (-0.6,+1.1)	-25.1 (-0.6,+1.2)	-24.8 (-0.8,+0.8)
QMIX	-33.3 (-11.6,+5.9)	-25.1 (-0.3,+0.6)	-39.5 (-0.8,+0.7)	-45.2 (-5.0,+5.0)	-47.0 (-3.2,+4.0)	-25.2 (-0.1,+0.1)	-28.9 (-1.6,+1.1)
	-59.6 (-0.5,+0.6)	-25.0 (-0.2,+0.3)	-39.3 (-1.2,+1.0)	-28.2 (-0.3,+0.3)	-27.5 (-0.4,+0.5)	-25.2 (-0.1,+0.1)	-28.1 (-0.7,+0.9)
IPPO	-	-	-	-	-	-	-
	-	-	-	-	-	-	-
MAPPO	-	-	-	-	-	-	-
	-	-	-	-	-	-	-

Fig. B.11. (SpeakerListener) Mean episodic returns for p_{default} at execution time.Fig. B.12. (SpeakerListener) Mean episodic returns for p_{default} during training.Fig. B.13. (SpeakerListener) Mean episodic returns for different p values at execution time.**Table B.12**(HearSee) Mean episodic returns for p_{default} at execution time.

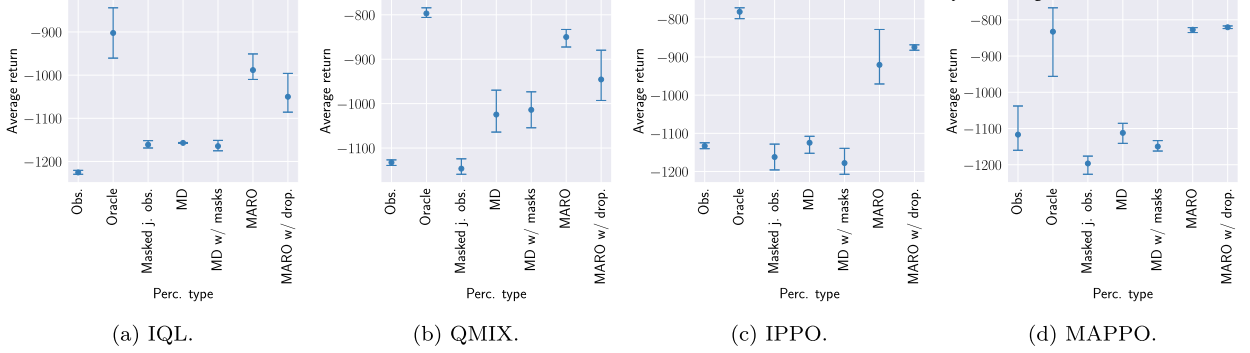
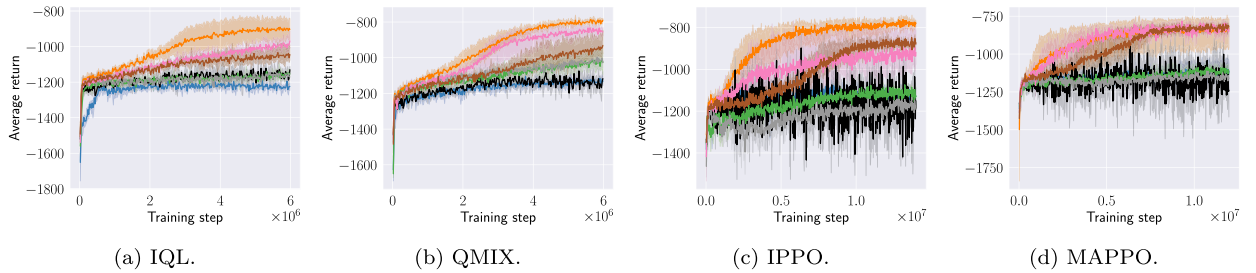
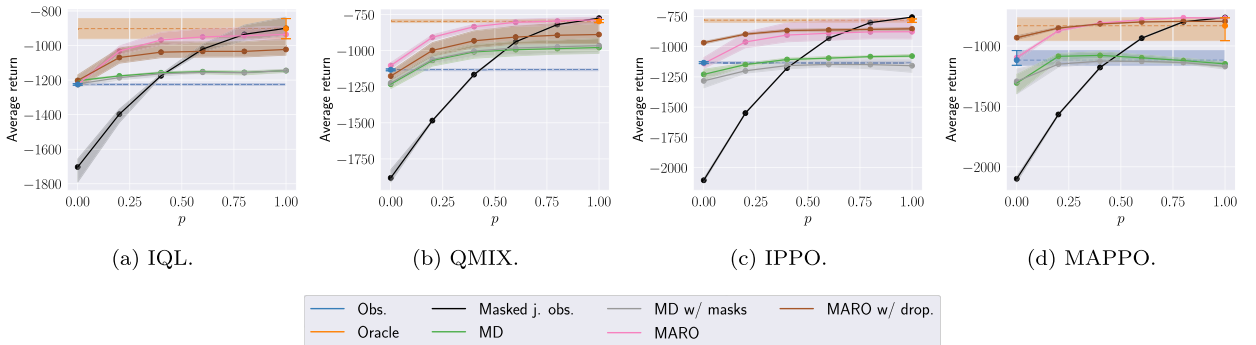
Algorithm	HearSee (p_{default})						
	Obs.	Oracle	Masked j. obs.	MD	MD w/ masks	MARO	MARO w/ drop.
IQL	-114.5 (-2.0,+1.6)	-24.5 (-0.6,+0.9)	-64.0 (-2.1,+2.5)	-34.8 (-1.6,+1.7)	-34.1 (-1.3,+2.5)	-29.6 (-1.0,+0.7)	-29.9 (-1.1,+0.6)
QMIX	-62.2 (-1.9,+1.4)	-23.6 (-0.7,+0.7)	-67.4 (-4.6,+3.0)	-29.2 (-1.3,+0.9)	-29.1 (-0.9,+0.8)	-28.8 (-1.2,+1.9)	-26.0 (-1.0,+0.8)
IPPO	-114.1 (-37.7,+27.7)	-25.7 (-0.2,+0.2)	-81.8 (-5.8,+7.0)	-102.9 (-20.9,+22.5)	-101.9 (-19.4,+20.1)	-31.4 (-1.4,+1.2)	-29.8 (-1.1,+1.6)
MAPPO	-70.5 (-18.3,+10.1)	-25.7 (-0.2,+0.2)	-82.2 (-6.4,+3.3)	-32.4 (-0.0,+0.0)	-30.9 (-3.5,+2.6)	-31.4 (-1.4,+1.2)	-28.7 (-1.4,+1.2)

Fig. B.14. (HearSee) Mean episodic returns for p_{default} at execution time.Fig. B.15. (HearSee) Mean episodic returns for p_{default} during training.Fig. B.16. (HearSee) Mean episodic returns for different p values at execution time.**Table B.13**(SpreadXY-2) Mean episodic returns for p_{default} at execution time.

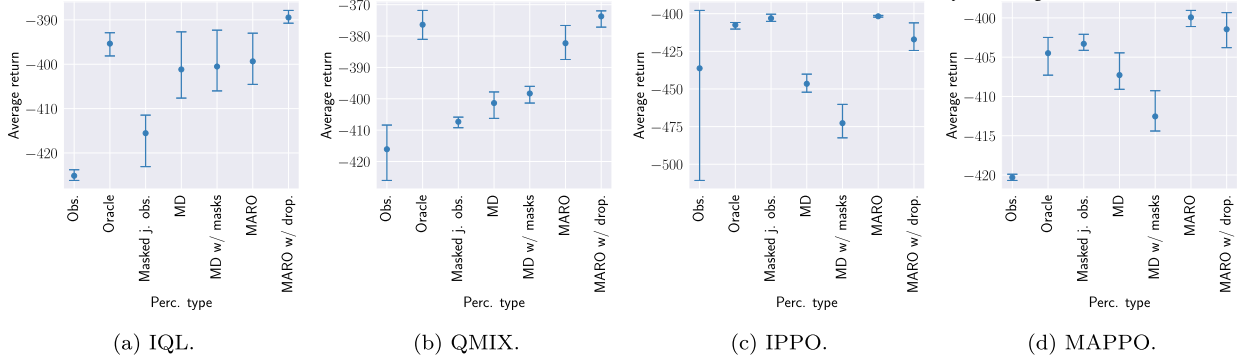
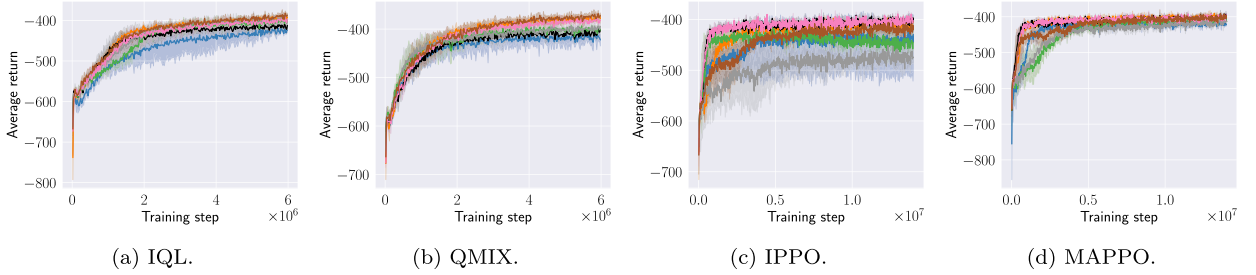
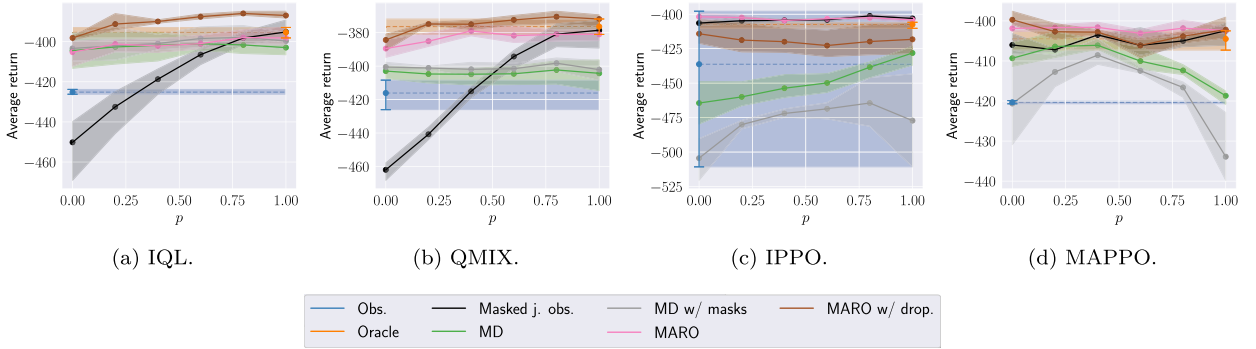
Algorithm	SpreadXY-2 (p_{default})						
	Obs.	Oracle	Masked j. obs.	MD	MD w/ masks	MARO	MARO w/ drop.
IQL	-199.6 (-0.9,+0.9)	-139.4 (-0.5,+0.6)	-202.9 (-2.3,+3.7)	-165.2 (-0.5,+0.7)	-160.7 (-1.7,+1.6)	-148.0 (-0.4,+0.5)	-158.8 (-1.2,+1.2)
QMIX	-177.8 (-7.6,+4.1)	-138.6 (-0.4,+0.4)	-201.2 (-2.3,+2.3)	-157.2 (-1.4,+0.7)	-154.5 (-0.5,+1.0)	-145.7 (-0.9,+0.5)	-152.7 (-0.5,+0.7)
IPPO	-235.6 (-0.6,+0.6)	-160.8 (-2.8,+1.4)	-214.8 (-5.4,+4.6)	-184.9 (-5.8,+3.6)	-175.9 (-3.0,+2.7)	-160.7 (-1.3,+1.0)	-166.6 (-1.0,+1.0)
MAPPO	-212.6 (-13.7,+24.5)	-160.8 (-1.8,+3.1)	-221.5 (-2.3,+3.2)	-181.1 (-3.9,+2.2)	-163.5 (-2.3,+2.7)	-161.2 (-0.9,+0.8)	-159.6 (-0.3,+0.3)

Fig. B.17. (SpreadXY-2) Mean episodic returns for p_{default} at execution time.Fig. B.18. (SpreadXY-2) Mean episodic returns for p_{default} during training.Fig. B.19. (SpreadXY-2) Mean episodic returns for different p values at execution time.**Table B.14**(SpreadXY-4) Mean episodic returns for p_{default} at execution time.

Algorithm	SpreadXY-4 (p_{default})							
	Obs.	Oracle	Masked j. obs.	MD	MD w/ masks	MARO	MARO w/ drop.	
IQL	-1225.5 (-4.2,+4.9)	-902.3 (-58.3,+58.3)	-1161.2 (-7.6,+9.4)	-1157.0 (-1.2,+1.0)	-1164.5 (-10.8,+13.3)	-988.3 (-21.7,+37.4)	-1050.1 (-35.7,+54.1)	
QMIX	-1132.6 (-6.6,+5.9)	-796.9 (-9.0,+12.7)	-1146.4 (-12.7,+22.1)	-1024.6 (-39.5,+54.9)	-1014.0 (-40.4,+40.6)	-850.0 (-22.5,+17.0)	-945.6 (-47.3,+65.9)	
IPPO	-1133.2 (-7.1,+8.4)	-781.6 (-18.0,+10.5)	-1162.1 (-33.8,+33.8)	-1124.7 (-27.6,+16.9)	-1177.9 (-29.4,+38.5)	-920.6 (-50.1,+92.7)	-874.6 (-7.7,+6.5)	
MAPPO	-1116.9 (-43.2,+79.0)	-832.8 (-)	-1196.5 (-29.8,+20.3)	-1112.1 (-28.9,+26.4)	-1149.7 (-12.5,+16.3)	-827.4 (-7.8,+5.8)	-820.6 (-3.6,+3.6)	

Fig. B.20. (SpreadXY-4) Mean episodic returns for p_{default} at execution time.Fig. B.21. (SpreadXY-4) Mean episodic returns for p_{default} during training.Fig. B.22. (SpreadXY-4) Mean episodic returns for different p values at execution time.**Table B.15**(SpreadBlindFold) Mean episodic returns for p_{default} at execution time.

Algorithm	SpreadBlindFold (p_{default})							
	Obs.	Oracle	Masked j. obs.	MD	MD w/ masks	MARO	MARO w/ drop.	
IQL	-425.1 (-1.1,+1.4)	-395.4 (-2.8,+2.5)	-415.5 (-7.5,+4.1)	-401.2 (-6.5,+8.5)	-400.5 (-5.5,+8.2)	-399.3 (-5.2,+6.4)	-389.5 (-1.3,+1.6)	
QMIX	-416.1 (-10.0,+7.7)	-376.4 (-4.7,+4.5)	-407.3 (-1.9,+1.5)	-401.4 (-4.9,+3.5)	-398.3 (-3.0,+2.3)	-382.3 (-5.2,+5.7)	-373.7 (-3.4,+1.8)	
IPPO	-436.3 (-74.5,+38.4)	-407.5 (-2.8,+1.6)	-403.1 (-2.1,+2.7)	-446.6 (-5.6,+6.4)	-472.7 (-9.7,+12.5)	-401.7 (-0.5,+0.6)	-417.1 (-7.4,+11.0)	
MAPPO	-420.3 (-0.4,+0.4)	-404.5 (-2.8,+2.0)	-403.3 (-0.8,+1.2)	-407.3 (-1.8,+2.8)	-412.5 (-1.9,+3.3)	-399.9 (-1.2,+0.9)	-401.4 (-2.3,+2.1)	

Fig. B.23. (SpreadBlindFold) Mean episodic returns for p_{default} at execution time.Fig. B.24. (SpreadBlindFold) Mean episodic returns for p_{default_t} during training.Fig. B.25. (SpreadBlindFold) Mean episodic returns for different p values at execution time.**Table B.16**

(Foraging-2s-15x15-2p-2f-coop-v2) Mean episodic returns at execution time.

Algorithm	Foraging-2s-15x15-2p-2f-coop-v2 (p_{default})							
	Obs.	Oracle	Masked j. obs.	MD	MD w/ masks	MARO	MARO w/ drop.	
IQL	0.38 (-0.03,+0.01)	0.48 (-0.03,+0.02)	0.19 (-0.02,+0.01)	0.53 (-0.03,+0.02)	0.52 (-0.02,+0.02)	0.35 (-0.01,+0.02)	0.52 (-0.01,+0.01)	
QMIX	0.55 (-0.01,+0.0)	0.68 (-0.02,+0.03)	0.25 (-0.05,+0.03)	0.58 (-0.01,+0.02)	0.59 (-0.02,+0.02)	0.44 (-0.02,+0.02)	0.60 (-0.01,+0.02)	
IPPO	0.31 (-0.0,+0.0)	0.44 (-0.0,+0.0)	0.30 (-0.01,+0.01)	0.03 (-0.02,+0.05)	0.01 (-0.01,+0.02)	0.37 (-0.01,+0.02)	0.01 (-0.0,+0.0)	
MAPPO	0.36 (-0.0,+0.0)	0.45 (-0.01,+0.01)	0.31 (-0.02,+0.03)	0.02 (-0.01,+0.02)	0.02 (-0.02,+0.03)	0.38 (-0.03,+0.04)	0.09 (-0.08,+0.06)	

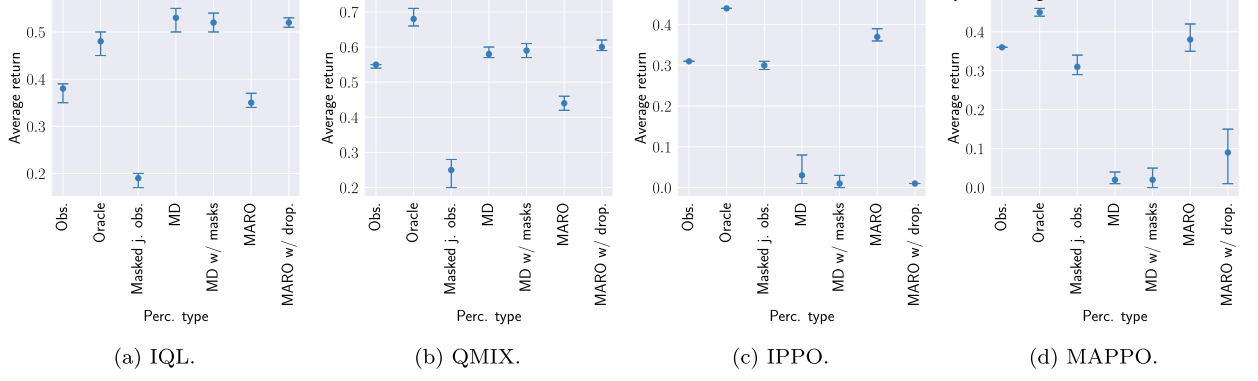


Fig. B.26. (Foraging-2s-15x15-2p-2f-coop-v2) Mean episodic returns at execution time.

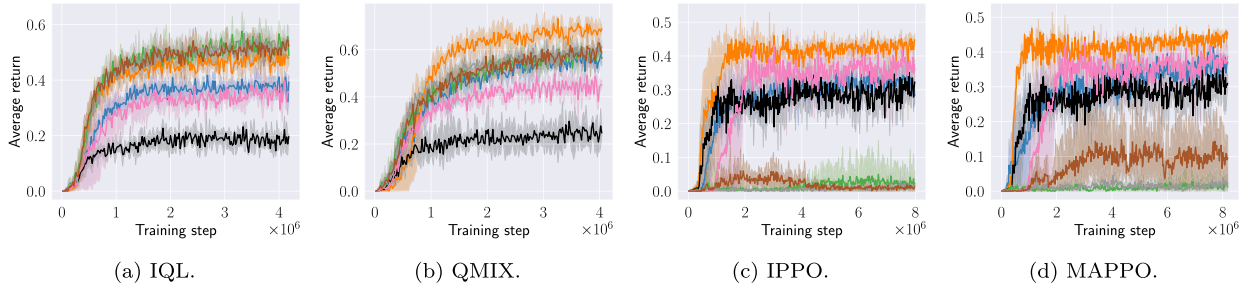
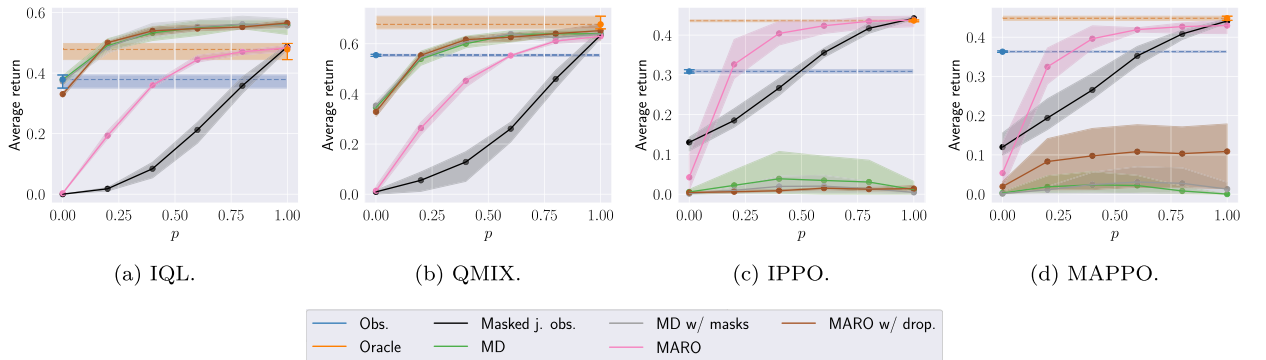


Fig. B.27. (Foraging-2s-15x15-2p-2f-coop-v2) Mean episodic returns during training.

Fig. B.28. (Foraging-2s-15x15-2p-2f-coop-v2) Mean episodic returns for different p values at execution time.

B.3.2. Sampling schemes of the communication matrix

In this section, we present the complete experimental results for the different sampling schemes of the communication matrix. The results herein presented correspond to the full results for Sec. 4.3.2 of the main text. More precisely, we display the mean episodic returns for: (i) the communication setting $p_{\text{asymmetric}}$, which features communication matrices C such that $p_{i,j} \neq p_{j,i} \sim \mathcal{U}(0, 1)$, sampled at the beginning of each episode; and (ii) the communication setting p_{dynamic} , similar to (i) but with C 's sampled every 5 time steps. The Oracle baseline is always evaluated with $p = 1$. (Tables B.17, B.18, Figs. B.29, B.30, Tables B.19, B.20, Figs. B.31, B.32, Tables B.21, B.22, Figs. B.33, B.34, Tables B.23, B.24, Figs. B.35, B.36, Tables B.25, B.26, Figs. B.37, B.38, Tables B.27, B.28, Figs. B.39, B.40.)

Table B.17(SpeakerListener) Mean episodic returns for $p_{\text{asymmetric}}$ at execution time.

Algorithm	SpeakerListener ($p_{\text{asymmetric}}$)						
	Obs.	Oracle	Masked j. obs.	MD	MD w/ masks	MARO	MARO w/ drop.
IQL	-40.0 (-0.4,+0.4)	-24.2 (-0.1,+0.2)	-45.6 (-1.4,+1.9)	-25.5 (-1.4,+1.1)	-25.6 (-1.4,+1.0)	-25.4 (-1.3,+1.0)	-25.4 (-1.3,+0.9)
QMIX	-24.9 (-0.1,+0.0)	-23.9 (-0.2,+0.2)	-40.4 (-0.4,+0.2)	-25.3 (-1.4,+1.0)	-25.3 (-1.5,+1.1)	-25.2 (-1.5,+1.1)	-24.5 (-0.4,+0.4)
IPPO	-33.3 (-11.6,+5.9)	-25.1 (-0.3,+0.6)	-36.9 (-0.1,+0.1)	-43.1 (-3.1,+3.1)	-44.8 (-2.0,+2.6)	-25.5 (-0.2,+0.3)	-29.0 (-1.0,+0.8)
MAPPO	-59.6 (-0.5,+0.6)	-25.0 (-0.2,+0.3)	-36.7 (-0.1,+0.2)	-28.8 (-0.1,+0.1)	-27.8 (-0.8,+0.8)	-25.5 (-0.2,+0.3)	-28.2 (-0.3,+0.6)

Table B.18(SpeakerListener) Mean episodic returns for p_{dynamic} at execution time.

Algorithm	SpeakerListener (p_{dynamic})						
	Obs.	Oracle	Masked j. obs.	MD	MD w/ masks	MARO	MARO w/ drop.
IQL	-40.0 (-0.4,+0.4)	-24.2 (-0.1,+0.2)	-44.8 (-1.6,+0.9)	-24.7 (-0.4,+0.3)	-24.8 (-0.4,+0.3)	-24.6 (-0.4,+0.4)	-24.6 (-0.3,+0.4)
QMIX	-24.9 (-0.1,+0.0)	-23.9 (-0.2,+0.2)	-39.7 (-1.1,+1.2)	-24.5 (-0.4,+0.3)	-24.5 (-0.3,+0.2)	-24.4 (-0.4,+0.2)	-24.5 (-0.2,+0.2)
IPPO	-33.3 (-11.6,+5.9)	-25.1 (-0.3,+0.6)	-35.7 (-0.1,+0.1)	-40.1 (-1.6,+1.6)	-40.5 (-2.2,+3.6)	-25.1 (-0.2,+0.2)	-28.7 (-1.0,+1.0)
MAPPO	-59.6 (-0.5,+0.6)	-25.0 (-0.2,+0.3)	-35.6 (-0.6,+0.3)	-27.8 (-0.2,+0.4)	-27.1 (-0.7,+0.8)	-25.1 (-0.2,+0.2)	-27.8 (-0.5,+0.7)

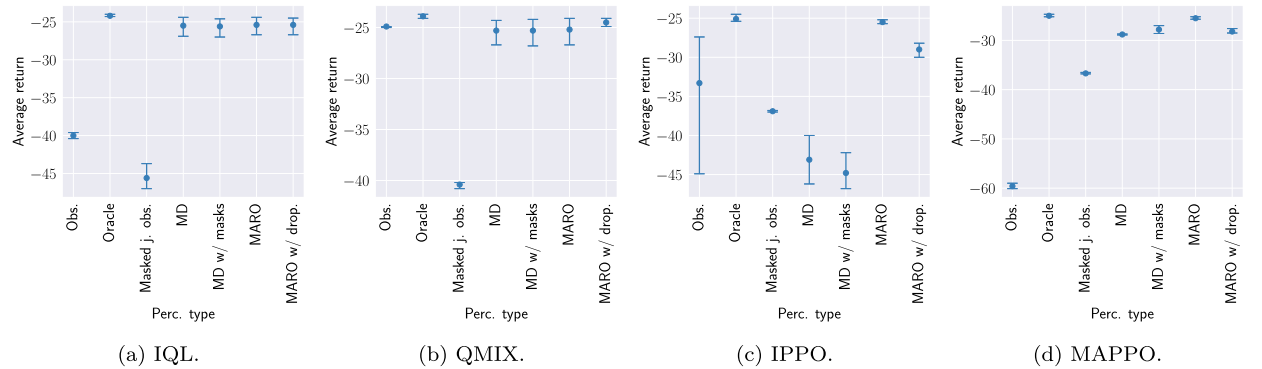
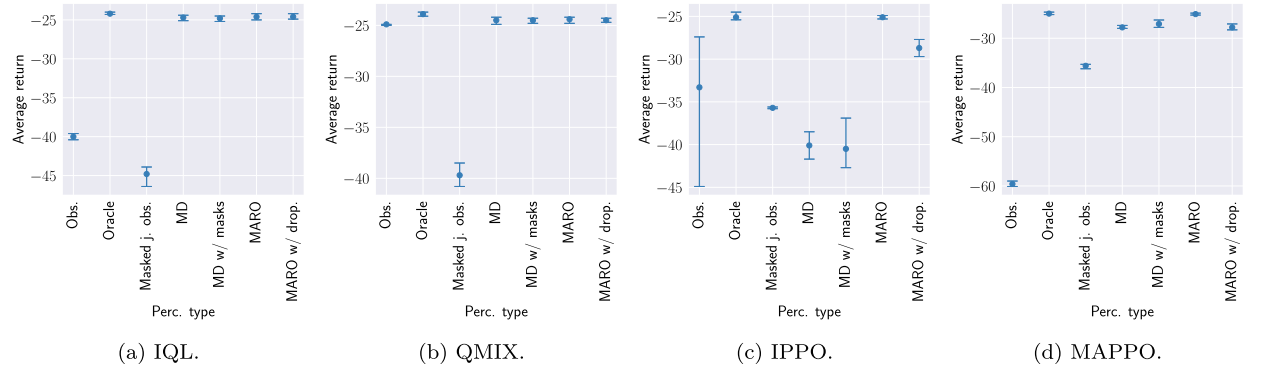
**Fig. B.29.** (SpeakerListener) Mean episodic returns for $p_{\text{asymmetric}}$ during training.**Fig. B.30.** (SpeakerListener) Mean episodic returns for p_{dynamic} during training.

Table B.19(HearSee) Mean episodic returns for $p_{\text{asymmetric}}$ at execution time.

Algorithm	HearSee ($p_{\text{asymmetric}}$)						
	Obs.	Oracle	Masked j. obs.	MD	MD w/ masks	MARO	MARO w/ drop.
IQL	-114.5 (-2.0,+1.6)	-24.5 (-0.6,+0.9)	-65.6 (-3.1,+4.5)	-35.7 (-1.1,+0.8)	-34.9 (-0.1,+0.1)	-30.9 (-1.8,+1.4)	-30.8 (-1.5,+0.9)
QMIX	-62.2 (-1.9,+1.4)	-23.6 (-0.7,+0.7)	-69.2 (-1.6,+1.0)	-30.5 (-0.1,+0.2)	-30.8 (-0.1,+0.3)	-29.9 (-1.1,+1.2)	-27.2 (-0.1,+0.2)
IPPO	-114.1 (-37.7,+27.7)	-25.7 (-0.2,+0.2)	-77.5 (-1.9,+2.0)	-98.2 (-25.1,+34.2)	-100.6 (-7.9,+11.5)	-33.4 (-2.0,+1.6)	-30.2 (-1.1,+1.5)
MAPPO	-70.5 (-18.3,+10.1)	-25.7 (-0.2,+0.2)	-79.1 (-1.4,+1.1)	-32.2 (-1.1,+1.2)	-30.4 (-1.0,+1.0)	-33.4 (-2.0,+1.6)	-29.0 (-1.4,+1.3)

Table B.20(HearSee) Mean episodic returns for p_{dynamic} at execution time.

Algorithm	HearSee (p_{dynamic})						
	Obs.	Oracle	Masked j. obs.	MD	MD w/ masks	MARO	MARO w/ drop.
IQL	-114.5 (-2.0,+1.6)	-24.5 (-0.6,+0.9)	-52.1 (-1.7,+3.0)	-33.0 (-0.5,+0.7)	-32.1 (-0.6,+0.9)	-28.5 (-0.5,+0.9)	-28.8 (-0.5,+0.5)
QMIX	-62.2 (-1.9,+1.4)	-23.6 (-0.7,+0.7)	-55.1 (-2.6,+2.3)	-29.1 (-0.3,+0.2)	-29.0 (-0.2,+0.3)	-27.5 (-1.2,+1.0)	-26.7 (-0.4,+0.3)
IPPO	-114.1 (-37.7,+27.7)	-25.7 (-0.2,+0.2)	-52.5 (-2.2,+3.4)	-84.8 (-27.8,+23.7)	-82.1 (-13.5,+9.8)	-27.5 (-1.2,+1.6)	-27.7 (-0.4,+0.7)
MAPPO	-70.5 (-18.3,+10.1)	-25.7 (-0.2,+0.2)	-53.3 (-1.2,+1.3)	-28.2 (-0.6,+0.9)	-26.8 (-0.4,+0.6)	-27.5 (-1.2,+1.6)	-26.6 (-1.0,+1.6)

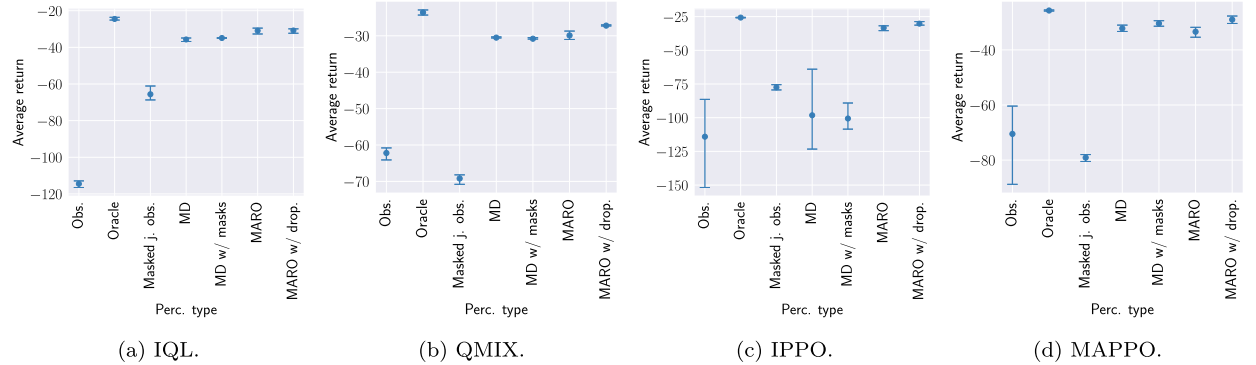
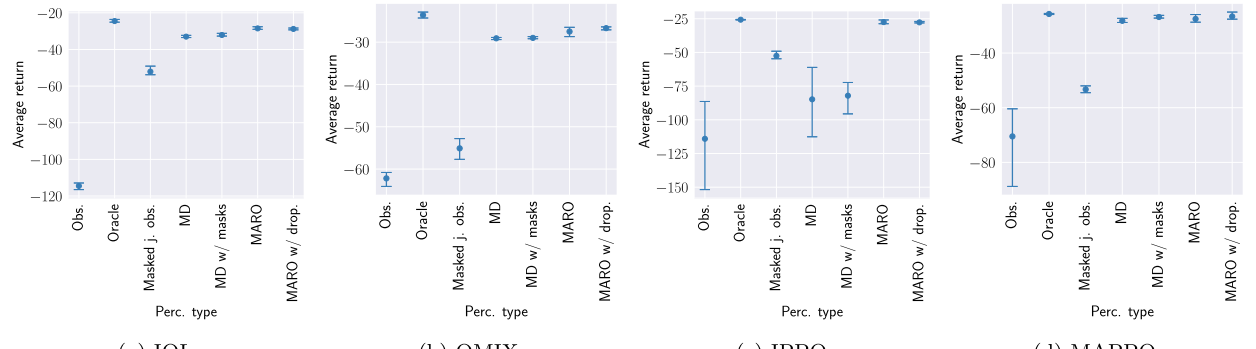
**Fig. B.31.** (HearSee) Mean episodic returns for $p_{\text{asymmetric}}$ during training.**Fig. B.32.** (HearSee) Mean episodic returns for p_{dynamic} during training.

Table B.21(SpreadXY-2) Mean episodic returns for $p_{\text{asymmetric}}$ at execution time.

Algorithm	Obs.	SpreadXY-2 ($p_{\text{asymmetric}}$)					
		Oracle	Masked j. obs.	MD	MD w/ masks	MARO	MARO w/ drop.
IQL	-199.6 (-0.9,+0.9)	-139.4 (-0.5,+0.6)	-200.2 (-0.5,+0.4)	-164.1 (-1.1,+0.7)	-160.5 (-0.8,+0.6)	-149.4 (-0.2,+0.3)	-158.3 (-0.8,+0.6)
QMIX	-177.8 (-7.6,+4.1)	-138.6 (-0.4,+0.4)	-197.9 (-1.0,+0.9)	-157.8 (-0.5,+0.2)	-154.3 (-1.3,+1.1)	-147.3 (-0.3,+0.3)	-152.7 (-0.8,+0.8)
IPPO	-235.6 (-0.6,+0.6)	-160.8 (-2.8,+1.4)	-205.4 (-3.5,+2.4)	-186.2 (-8.7,+5.5)	-175.0 (-1.1,+1.3)	-161.1 (-2.0,+1.1)	-166.8 (-0.2,+0.3)
MAPPO	-212.6 (-13.7,+24.5)	-160.8 (-1.8,+3.1)	-209.4 (-1.9,+1.1)	-184.0 (-3.2,+1.9)	-165.7 (-3.7,+2.4)	-161.2 (-0.4,+0.3)	-160.6 (-1.0,+0.8)

Table B.22(SpreadXY-2) Mean episodic returns for p_{dynamic} at execution time.

Algorithm	Obs.	SpreadXY-2 (p_{dynamic})					
		Oracle	Masked j. obs.	MD	MD w/ masks	MARO	MARO w/ drop.
IQL	-199.6 (-0.9,+0.9)	-139.4 (-0.5,+0.6)	-196.7 (-2.3,+2.2)	-161.2 (-0.4,+0.3)	-157.6 (-0.8,+0.8)	-145.3 (-1.0,+1.5)	-155.7 (-0.4,+0.6)
QMIX	-177.8 (-7.6,+4.1)	-138.6 (-0.4,+0.4)	-193.7 (-1.4,+2.1)	-155.8 (-0.8,+0.4)	-152.6 (-0.7,+1.2)	-143.5 (-1.1,+1.9)	-150.2 (-0.8,+0.8)
IPPO	-235.6 (-0.6,+0.6)	-160.8 (-2.8,+1.4)	-200.8 (-2.2,+2.5)	-183.5 (-7.9,+4.7)	-171.3 (-1.4,+0.7)	-157.3 (-0.5,+0.3)	-166.7 (-1.2,+0.9)
MAPPO	-212.6 (-13.7,+24.5)	-160.8 (-1.8,+3.1)	-203.3 (-2.4,+1.7)	-179.6 (-3.3,+2.3)	-162.9 (-2.5,+2.1)	-157.7 (-0.3,+0.3)	-158.8 (-0.6,+0.4)

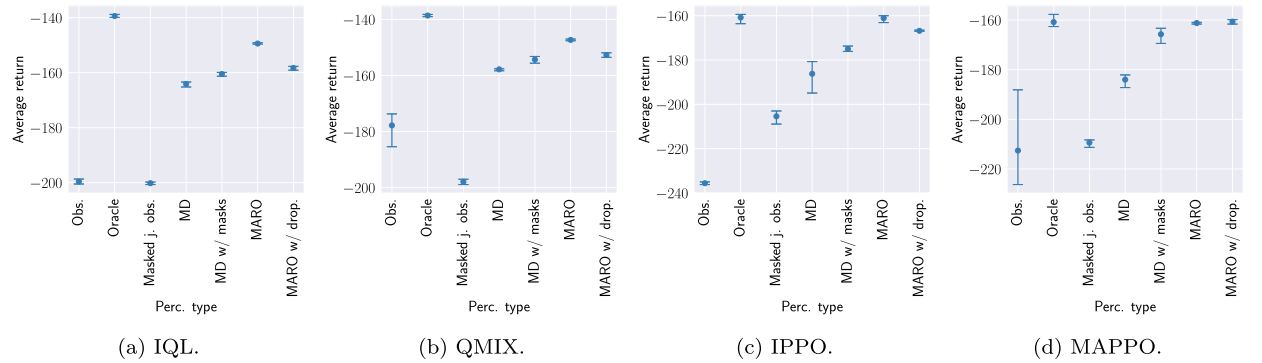
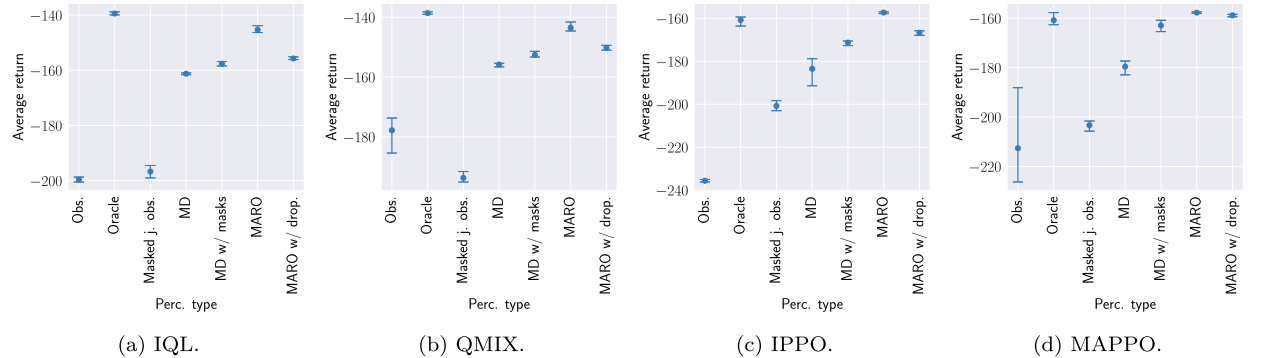
**Fig. B.33.** (SpreadXY-2) Mean episodic returns for $p_{\text{asymmetric}}$ during training.**Fig. B.34.** (SpreadXY-2) Mean episodic returns for p_{dynamic} during training.

Table B.23(SpreadXY-4) Mean episodic returns for $p_{\text{asymmetric}}$ at execution time.

Algorithm	Obs.	SpreadXY-4 ($p_{\text{asymmetric}}$)					
		Oracle	Masked j. obs.	MD	MD w/ masks	MARO	MARO w/ drop.
IQL	-1225.5 (-4.2,+4.9)	-902.3 (-58.3,+58.3)	-1126.1 (-16.4,+14.8)	-1166.3 (-6.8,+9.1)	-1168.8 (-9.5,+7.3)	-983.9 (-34.5,+44.3)	-1054.5 (-31.5,+55.7)
QMIX	-1132.6 (-6.6,+5.9)	-796.9 (-9.0,+12.7)	-1080.0 (-12.0,+8.8)	-1030.4 (-42.9,+58.2)	-1020.5 (-36.9,+44.2)	-852.9 (-24.0,+20.0)	-945.6 (-46.5,+64.7)
IPPO	-1133.2 (-7.1,+8.4)	-781.6 (-18.0,+10.5)	-1062.8 (-10.1,+10.1)	-1110.5 (-16.3,+14.7)	-1162.0 (-27.8,+44.8)	-915.8 (-2.4,+104.8)	-869.2 (-10.9,+10.3)
MAPPO	-1116.9 (-43.2,+79.0)	-832.8 (-23.2,+28.7)	-1066.9 (-23.2,+28.7)	-1128.1 (-26.2,+20.1)	-1160.7 (-12.0,+13.1)	-823.9 (-1.9,+1.8)	-827.8 (-7.0,+7.5)

Table B.24(SpreadXY-4) Mean episodic returns for p_{dynamic} at execution time.

Algorithm	Obs.	SpreadXY-4 (p_{dynamic})					
		Oracle	Masked j. obs.	MD	MD w/ masks	MARO	MARO w/ drop.
IQL	-1225.5 (-4.2,+4.9)	-902.3 (-58.3,+58.3)	-1114.9 (-12.4,+6.7)	-1161.7 (-4.9,+3.8)	-1165.9 (-7.9,+4.1)	-971.8 (-27.0,+40.3)	-1041.3 (-32.3,+54.4)
QMIX	-1132.6 (-6.6,+5.9)	-796.9 (-9.0,+12.7)	-1069.5 (-2.7,+5.0)	-1016.4 (-38.6,+58.4)	-1006.9 (-40.3,+43.3)	-833.4 (-25.9,+19.9)	-932.2 (-46.6,+70.9)
IPPO	-1133.2 (-7.1,+8.4)	-781.6 (-18.0,+10.5)	-1077.0 (-8.2,+8.2)	-1097.3 (-18.2,+16.0)	-1155.6 (-26.5,+38.9)	-904.6 (-26.0,+101.7)	-863.6 (-6.9,+10.1)
MAPPO	-1116.9 (-43.2,+79.0)	-832.8 (-23.2,+4.4)	-1068.3 (-2.7,+4.4)	-1101.7 (-32.2,+23.5)	-1136.7 (-13.5,+16.8)	-813.0 (-3.4,+2.9)	-813.8 (-2.6,+3.7)

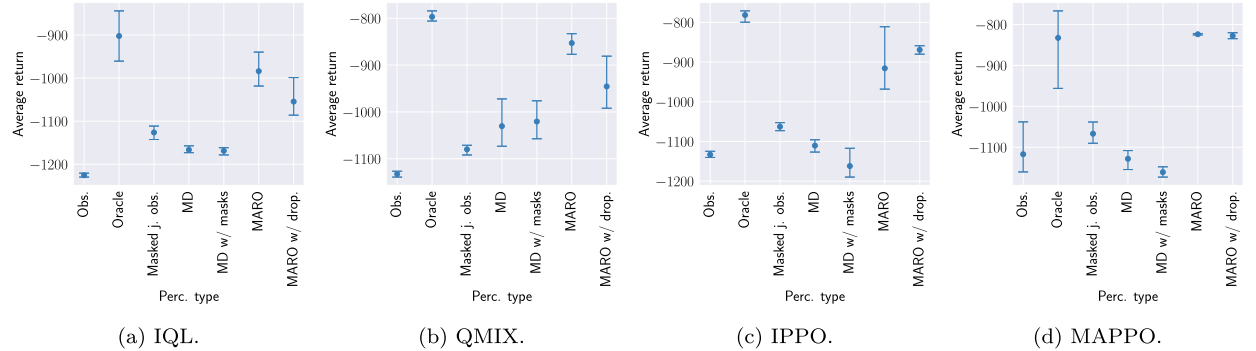
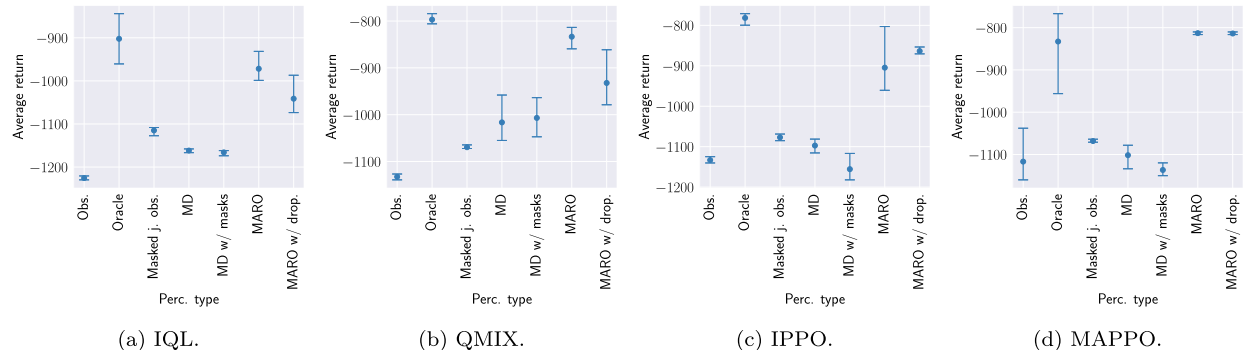
**Fig. B.35.** (SpreadXY-4) Mean episodic returns for $p_{\text{asymmetric}}$ during training.**Fig. B.36.** (SpreadXY-4) Mean episodic returns for p_{dynamic} during training.

Table B.25(SpreadBlindFold) Mean episodic returns for $p_{\text{asymmetric}}$ at execution time.

Algorithm	SpreadBlindFold ($p_{\text{asymmetric}}$)						
	Obs.	Oracle	Masked j. obs.	MD	MD w/ masks	MARO	MARO w/ drop.
IQL	-425.1 (-1.1,+1.4)	-395.4 (-2.8,+2.5)	-414.6 (-6.4,+5.3)	-402.7 (-6.5,+3.4)	-398.5 (-1.6,+2.2)	-400.5 (-3.4,+3.0)	-390.0 (-0.7,+0.6)
QMIX	-416.1 (-10.0,+7.7)	-376.4 (-4.7,+4.5)	-407.3 (-6.8,+6.6)	-403.7 (-8.4,+4.4)	-401.0 (-6.6,+5.0)	-380.8 (-2.1,+3.3)	-373.5 (-6.0,+3.6)
IPPO	-436.3 (-74.5,+38.4)	-407.5 (-2.8,+1.6)	-402.1 (-1.2,+2.4)	-447.7 (-5.8,+5.5)	-473.0 (-11.7,+7.7)	-403.4 (-0.7,+1.3)	-420.5 (-9.9,+12.3)
MAPPO	-420.3 (-0.4,+0.4)	-404.5 (-2.8,+2.0)	-403.3 (-1.7,+1.5)	-409.6 (-2.9,+3.5)	-412.3 (-2.1,+2.1)	-401.4 (-2.1,+1.8)	-402.6 (-2.3,+2.2)

Table B.26(SpreadBlindFold) Mean episodic returns for p_{dynamic} at execution time.

Algorithm	SpreadBlindFold (p_{dynamic})						
	Obs.	Oracle	Masked j. obs.	MD	MD w/ masks	MARO	MARO w/ drop.
IQL	-425.1 (-1.1,+1.4)	-395.4 (-2.8,+2.5)	-411.9 (-6.4,+4.5)	-403.0 (-7.9,+7.5)	-397.8 (-4.6,+7.7)	-401.4 (-2.4,+4.4)	-389.3 (-1.5,+0.9)
QMIX	-416.1 (-10.0,+7.7)	-376.4 (-4.7,+4.5)	-404.6 (-2.7,+2.0)	-402.7 (-6.7,+3.5)	-398.6 (-4.2,+4.5)	-381.9 (-5.0,+5.6)	-372.0 (-3.9,+2.7)
IPPO	-436.3 (-74.5,+38.4)	-407.5 (-2.8,+1.6)	-403.6 (-1.5,+1.3)	-447.3 (-8.6,+8.7)	-470.4 (-5.0,+9.3)	-404.4 (-1.1,+1.1)	-418.7 (-7.6,+10.6)
MAPPO	-420.3 (-0.4,+0.4)	-404.5 (-2.8,+2.0)	-405.4 (-2.0,+1.4)	-408.1 (-2.4,+3.7)	-411.1 (-1.9,+1.8)	-404.1 (-2.1,+2.9)	-403.0 (-2.0,+1.5)

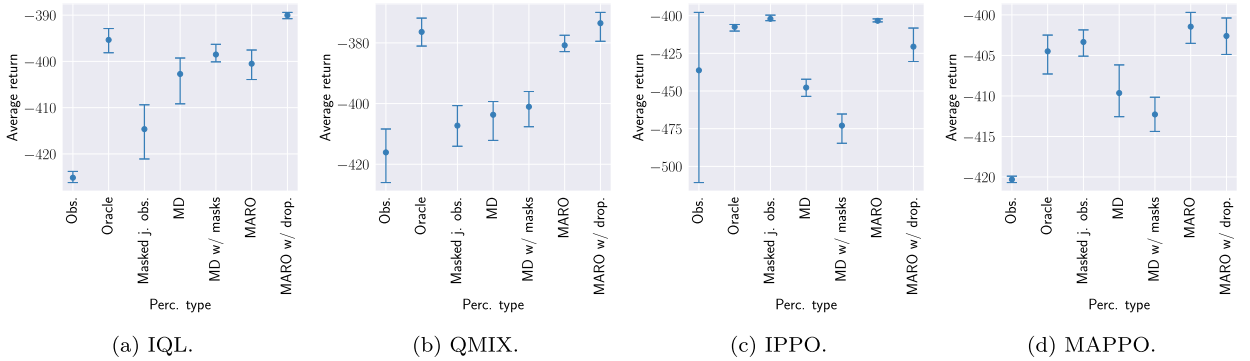
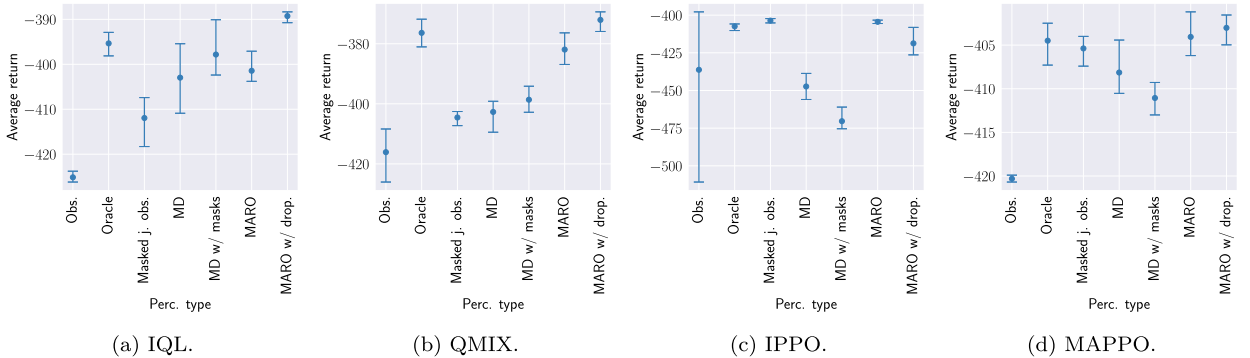
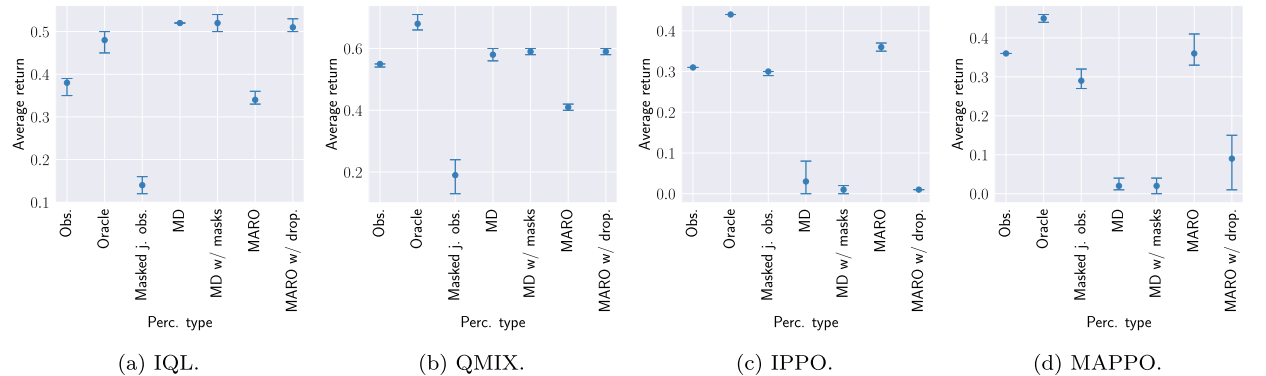
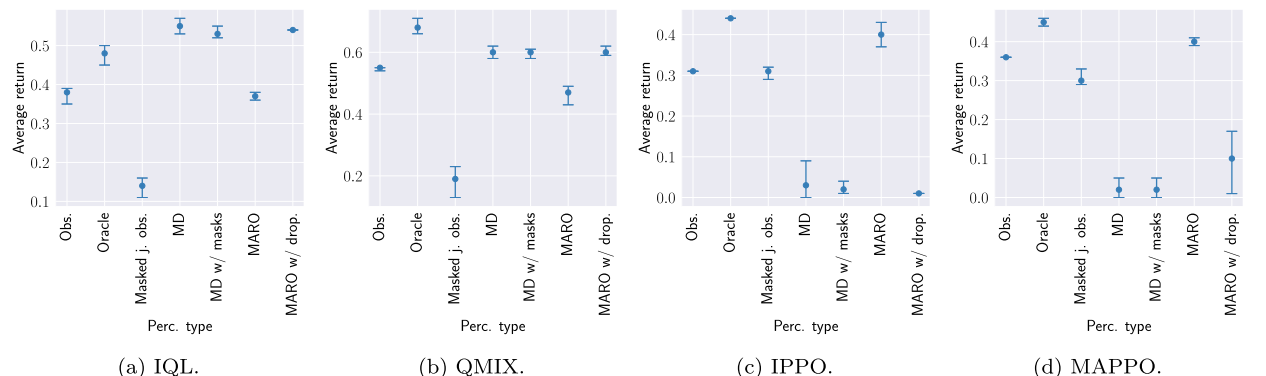
**Fig. B.37.** (SpreadBlindFold) Mean episodic returns for $p_{\text{asymmetric}}$ during training.**Fig. B.38.** (SpreadBlindFold) Mean episodic returns for p_{dynamic} during training.

Table B.27(Foraging-2s-15x15-2p-2f-coop-v2) Mean returns for p_{asym} at execution time.

Algorithm	Foraging-2s-15x15-2p-2f-coop-v2 ($p_{\text{asymmetric}}$)						
	Obs.	Oracle	Masked j. obs.	MD	MD w/ masks	MARO	MARO w/ drop.
IQL	0.38 (-0.03,+0.01)	0.48 (-0.03,+0.02)	0.14 (-0.02,+0.02)	0.52 (-0.0,+0.0)	0.52 (-0.02,+0.02)	0.34 (-0.01,+0.02)	0.51 (-0.01,+0.02)
QMIX	0.55 (-0.01,+0.0)	0.68 (-0.02,+0.03)	0.19 (-0.06,+0.05)	0.58 (-0.02,+0.02)	0.59 (-0.01,+0.01)	0.41 (-0.01,+0.01)	0.59 (-0.01,+0.01)
IPPO	0.31 (-0.0,+0.0)	0.44 (-0.0,+0.0)	0.3 (-0.01,+0.0)	0.03 (-0.03,+0.05)	0.01 (-0.01,+0.01)	0.36 (-0.01,+0.01)	0.01 (-0.0,+0.0)
MAPPO	0.36 (-0.0,+0.0)	0.45 (-0.01,+0.01)	0.29 (-0.02,+0.03)	0.02 (-0.01,+0.02)	0.02 (-0.02,+0.02)	0.36 (-0.03,+0.05)	0.09 (-0.08,+0.06)

Table B.28(Foraging-2s-15x15-2p-2f-coop-v2) Mean returns for p_{dyn} at execution time.

Algorithm	Foraging-2s-15x15-2p-2f-coop-v2 (p_{dynamic})						
	Obs.	Oracle	Masked j. obs.	MD	MD w/ masks	MARO	MARO w/ drop.
IQL	0.38 (-0.03,+0.01)	0.48 (-0.03,+0.02)	0.14 (-0.03,+0.02)	0.55 (-0.02,+0.02)	0.53 (-0.01,+0.02)	0.37 (-0.01,+0.01)	0.54 (-0.0,+0.0)
QMIX	0.55 (-0.01,+0.0)	0.68 (-0.02,+0.03)	0.19 (-0.06,+0.04)	0.6 (-0.02,+0.02)	0.6 (-0.02,+0.01)	0.47 (-0.04,+0.02)	0.6 (-0.01,+0.02)
IPPO	0.31 (-0.0,+0.0)	0.44 (-0.0,+0.0)	0.31 (-0.02,+0.01)	0.03 (-0.03,+0.06)	0.02 (-0.01,+0.02)	0.4 (-0.03,+0.03)	0.01 (-0.0,+0.0)
MAPPO	0.36 (-0.0,+0.0)	0.45 (-0.01,+0.01)	0.3 (-0.01,+0.03)	0.02 (-0.02,+0.03)	0.02 (-0.02,+0.03)	0.4 (-0.01,+0.01)	0.1 (-0.09,+0.07)

**Fig. B.39.** (Foraging-2s-15x15-2p-2f-coop-v2) Mean episodic returns for $p_{\text{asymmetric}}$ during training.**Fig. B.40.** (Foraging-2s-15x15-2p-2f-coop-v2) Mean episodic returns for p_{dynamic} during training.

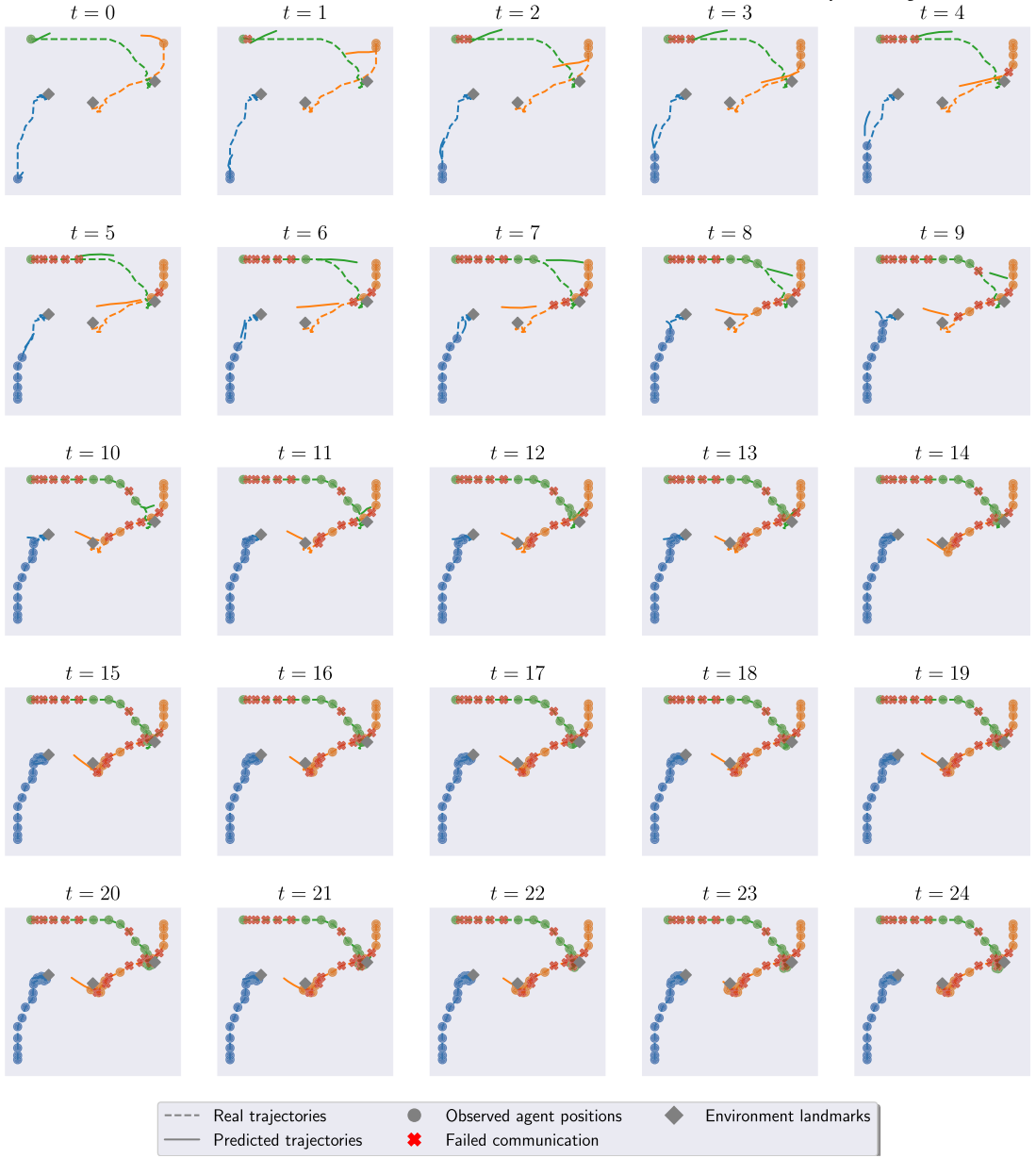


Fig. B.41. Trajectory prediction plots for the Spreadblindfold environment under the QMIX algorithm from the perspective of agent 0 (blue). (For interpretation of the colors in the figure(s), the reader is referred to the web version of this article.)

B.3.3. Multi-agent trajectory prediction

We display, in Figs. B.41, B.42 and B.43, an illustration of the trajectory predictions made by the predictive model from the perspective of each of the agents. The plots are computed, at each timestep and from the perspective of each agent, by computing the estimated trajectories of all agents for the next 4 timesteps. The 4-step ahead predictions are entirely computed using estimated quantities, i.e., real observations are not incorporated into the predictions and the predictive model works in a fully auto-regressive manner.

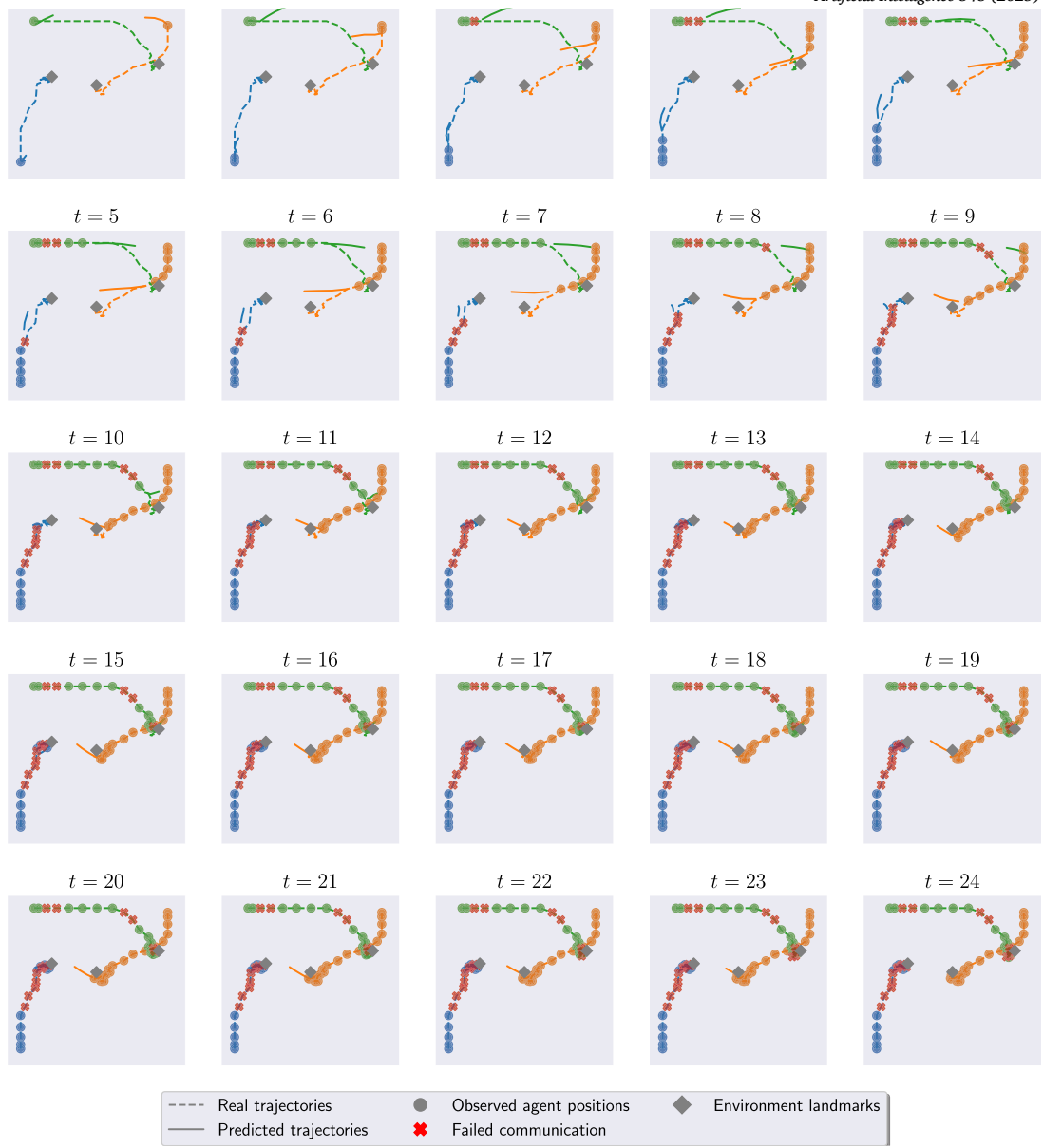


Fig. B.42. Trajectory prediction plots for the Spreadblindfold environment under the QMIX algorithm from the perspective of agent 1 (orange). (For interpretation of the colors in the figure(s), the reader is referred to the web version of this article.)

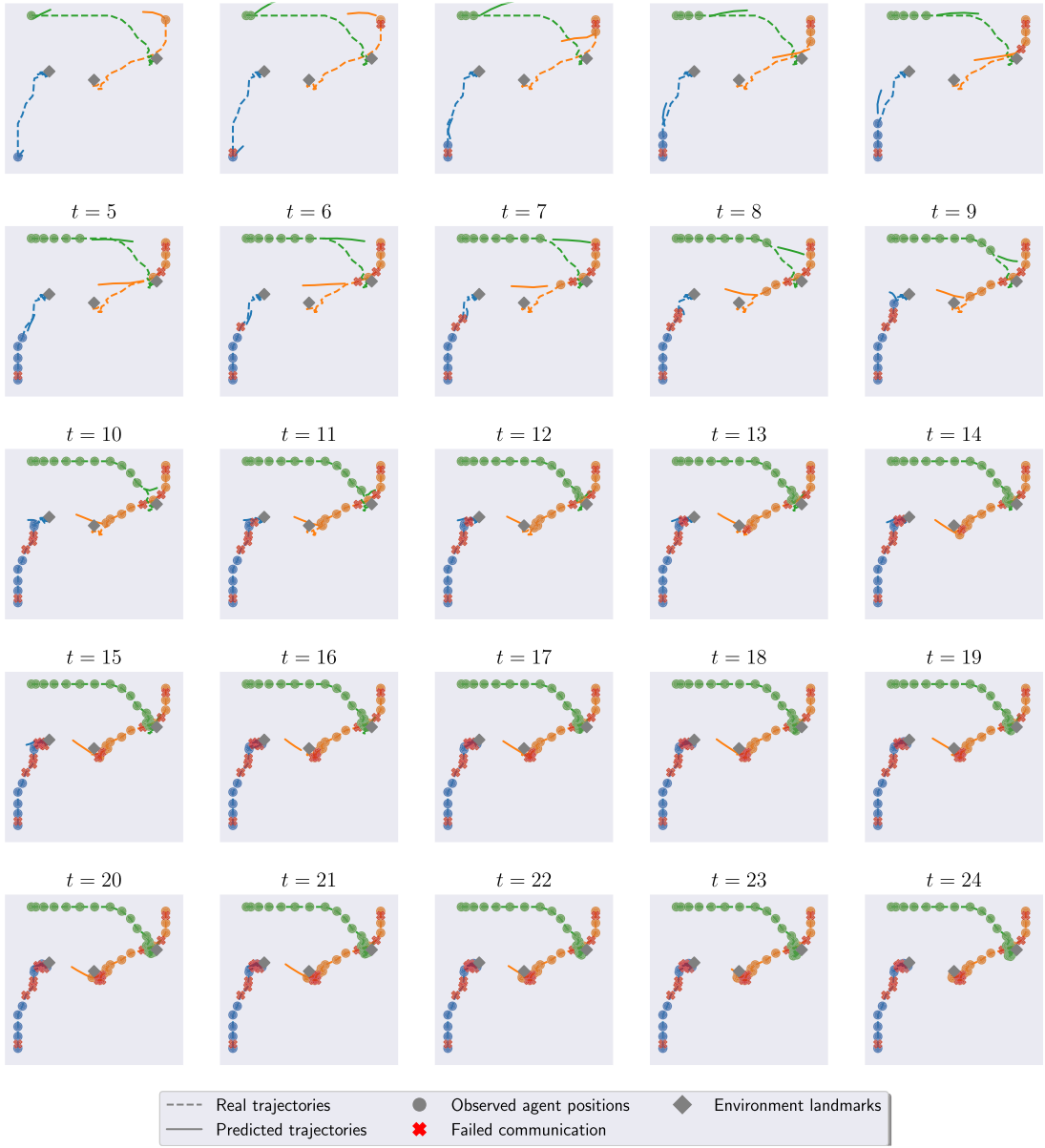


Fig. B.43. Trajectory prediction plots for the Spreadblindfold environment under the QMIX algorithm from the perspective of agent 2 (green). (For interpretation of the colors in the figure(s), the reader is referred to the web version of this article.)

Data availability

The article contains a link to a GitHub repository containing all the code used in the experiments.

References

- [1] G. Papoudakis, F. Christianos, L. Schäfer, S.V. Albrecht, Comparative evaluation of multi-agent deep reinforcement learning algorithms, CoRR, arXiv:2006.07869, 2020.
- [2] H. Wei, G. Zheng, V.V. Gayah, Z. Li, A survey on traffic signal control methods, CoRR, arXiv:1904.08117, 2019.
- [3] X. Fang, J. Wang, G. Song, Y. Han, Q. Zhao, Z. Cao, Multi-agent reinforcement learning approach for residential microgrid energy scheduling, Energies 13 (1) (2020).
- [4] L. Canese, G.C. Cardarilli, L. Di Nunzio, R. Fazzolari, D. Giardino, M. Re, S. Spanò, Multi-agent reinforcement learning: a review of challenges and applications, Appl. Sci. 11 (11) (2021).
- [5] F.A. Oliehoek, M.T.J. Spaan, N. Vlassis, Optimal and approximate q-value functions for decentralized pomdps, CoRR, arXiv:1111.0062, 2011.
- [6] T. Rashid, M. Samvelyan, C.S. de Witt, G. Farquhar, J.N. Foerster, S. Whiteson, QMIX: monotonic value function factorisation for deep multi-agent reinforcement learning, CoRR, arXiv:1803.11485, 2018.

- [7] J.N. Foerster, Y.M. Assael, N. de Freitas, S. Whiteson, Learning to communicate with deep multi-agent reinforcement learning, CoRR, arXiv:1605.06676, 2016.
- [8] F. Ho, A. Salta, R. Geraldes, A. Goncalves, M. Cavazza, H. Prendinger, Multi-agent path finding for uav traffic management, in: Proceedings of the 18th International Conference on Autonomous Agents and MultiAgent Systems, 2019, pp. 131–139.
- [9] E. Yurtsever, J. Lambert, A. Carballo, K. Takeda, A survey of autonomous driving: common practices and emerging technologies, IEEE Access 8 (2020) 58443–58469.
- [10] C. Zhu, M. Dastani, S. Wang, A survey of multi-agent reinforcement learning with communication, <https://doi.org/10.48550/ARXIV.2203.08975>, 2022.
- [11] P.P. Santos, D.S. Carvalho, M. Vasco, A. Sardinha, P.A. Santos, A. Paiva, F.S. Melo, Centralized training with hybrid execution in multi-agent reinforcement learning: extended abstract, in: Proc. of the 23rd International Conference on Autonomous Agents and Multiagent Systems (AAMAS), Auckland, New Zealand, 2024.
- [12] F.A. Oliehoek, C. Amato, A Concise Introduction to Decentralized POMDPs, Springer, 2016.
- [13] M. Tan, Multi-agent reinforcement learning: independent vs. cooperative agents, in: Proceedings of the Tenth International Conference on Machine Learning, 1993, pp. 330–337.
- [14] J. Schulman, F. Wolski, P. Dhariwal, A. Radford, O. Klimov, Proximal policy optimization algorithms, arXiv:1707.06347, 2017.
- [15] C. Yu, A. Veliu, E. Vinitsky, Y. Wang, A.M. Bayen, Y. Wu, The surprising effectiveness of MAPPO in cooperative, multi-agent games, CoRR, arXiv:2103.01955 [abs], 2021, arXiv:2103.01955.
- [16] S. Omidshafiei, D. Hennes, M. Garnelo, E. Tarassov, Z. Wang, R. Elie, J.T. Connor, P. Muller, I. Graham, W. Spearman, K. Tuyls, Time-series imputation of temporally-occluded multiagent trajectories, CoRR, arXiv:2106.04219, 2021.
- [17] G. Papoudakis, F. Christianos, L. Schäfer, S.V. Albrecht, Benchmarking multi-agent deep reinforcement learning algorithms in cooperative tasks, in: Thirty-Fifth Conference on Neural Information Processing Systems Datasets and Benchmarks Track, 2021 (Round 1).
- [18] R. Lowe, Y.I. Wu, A. Tamar, J. Harb, O. Pieter Abbeel, I. Mordatch, Multi-agent actor-critic for mixed cooperative-competitive environments, Adv. Neural Inf. Process. Syst. 30 (2017).
- [19] W. Kim, M. Cho, Y. Sung, Message-dropout: an efficient training method for multi-agent deep reinforcement learning, CoRR, arXiv:1902.06527, 2019.
- [20] S. Omidshafiei, J. Pazis, C. Amato, J.P. How, J. Vian, Deep decentralized multi-task multi-agent reinforcement learning under partial observability, in: Proceedings of the 34th International Conference on Machine Learning, 2017, pp. 2681–2690.
- [21] W. Mao, K. Zhang, E. Miehling, T. Basar, Information state embedding in partially observable cooperative multi-agent reinforcement learning, CoRR, arXiv: 2004.01098, 2020.
- [22] J.N. Foerster, G. Farquhar, T. Afouras, N. Nardelli, S. Whiteson, Counterfactual multi-agent policy gradients, CoRR, arXiv:1705.08926, 2017.
- [23] Y. Niu, R. Paleja, M. Gombolay, Multi-agent graph-attention communication and teaming, in: Proceedings of the 20th International Conference on Autonomous Agents and MultiAgent Systems, 2021, pp. 964–973.
- [24] D. Kim, S. Moon, D. Hostallero, W.J. Kang, T. Lee, K. Son, Y. Yi, Learning to schedule communication in multi-agent reinforcement learning, CoRR, arXiv: 1902.01554, 2019.
- [25] A. Singh, T. Jain, S. Sukhbaatar, Learning when to communicate at scale in multiagent cooperative and competitive tasks, CoRR, arXiv:1812.09755, 2018.
- [26] G. Hu, Y. Zhu, D. Zhao, M. Zhao, J. Hao, Event-triggered multi-agent reinforcement learning with communication under limited-bandwidth constraint, CoRR, arXiv:2010.04978, 2020.
- [27] R. Wang, X. He, R. Yu, W. Qiu, B. An, Z. Rabinovich, Learning efficient multi-agent communication: an information bottleneck approach, CoRR, arXiv:1911.06992, 2019.
- [28] S.Q. Zhang, Q. Zhang, J. Lin, Efficient communication in multi-agent reinforcement learning via variance based control, CoRR, arXiv:1909.02682, 2019.
- [29] S.Q. Zhang, J. Lin, Q. Zhang, Succinct and robust multi-agent communication with temporal message control, CoRR, arXiv:2010.14391, 2020.
- [30] R.E. Wang, M. Everett, J.P. How, R-MADDPG for partially observable environments and limited communication, CoRR, arXiv:2002.06684, 2020.
- [31] G. Papoudakis, F. Christianos, S. Albrecht, Agent modelling under partial observability for deep reinforcement learning, Adv. Neural Inf. Process. Syst. 34 (2021) 19210–19222.
- [32] A. Xie, D.P. Losey, R. Tolsma, C. Finn, D. Sadigh, Learning latent representations to influence multi-agent interaction, arXiv preprint, arXiv:2011.06619, 2020.
- [33] H. He, J. Boyd-Graber, K. Kwok, H. Daumé III, Opponent modeling in deep reinforcement learning, in: International Conference on Machine Learning, PMLR, 2016, pp. 1804–1813.
- [34] A. Alahi, K. Goel, V. Ramanathan, A. Robicquet, L. Fei-Fei, S. Savarese, Social lstm: human trajectory prediction in crowded spaces, in: 2016 IEEE Conference on Computer Vision and Pattern Recognition (CVPR), 2016.
- [35] R.A. Yeh, A.G. Schwing, J. Huang, K. Murphy, Diverse generation for multi-agent sports games, in: 2019 IEEE/CVF Conference on Computer Vision and Pattern Recognition (CVPR), 2019, pp. 4605–4614.
- [36] S. Hauri, N. Djuric, V. Radostavljevic, S. Vucetic, Multi-modal trajectory prediction of NBA players, CoRR, arXiv:2008.07870, 2020.
- [37] E. Bargiacchi, T. Verstraeten, D.M. Roijers, Cooperative prioritized sweeping, in: Proceedings of the 20th International Conference on Autonomous Agents and MultiAgent Systems, 2021, pp. 160–168.
- [38] W. Kim, J. Park, Y. Sung, Communication in multi-agent reinforcement learning: intention sharing, in: International Conference on Learning Representations, 2021.
- [39] X. Wang, Z. Zhang, W. Zhang, Model-based multi-agent reinforcement learning: recent progress and prospects, <https://doi.org/10.48550/ARXIV.2203.10603>, 2022.
- [40] S. Sukhbaatar, A. Szlam, R. Fergus, Learning multiagent communication with backpropagation, CoRR, arXiv:1605.07736, 2016.
- [41] J. Jiang, Z. Lu, Learning attentional communication for multi-agent cooperation, CoRR, arXiv:1805.07733, 2018.
- [42] D. Willemsen, M. Coppola, G.C. de Croon Mambpo, Sample-efficient multi-robot reinforcement learning using learned world models, in: 2021 IEEE/RSJ International Conference on Intelligent Robots and Systems (IROS), 2021, pp. 5635–5640.
- [43] A. Paszke, S. Gross, F. Massa, A. Lerer, J. Bradbury, G. Chanan, T. Killeen, Z. Lin, N. Gimelshein, L. Antiga, A. Desmaison, A. Kopf, E. Yang, Z. DeVito, M. Raison, A. Tejani, S. Chilamkurthy, B. Steiner, L. Fang, J. Bai, S. Chintala, Pytorch: an imperative style, high-performance deep learning library, in: Advances in Neural Information Processing Systems, vol. 32, 2019, pp. 8024–8035.